X-Mahalanobis: Transformer Feature Mixing for Reliable OOD Detection

 $\begin{array}{cccc} \textbf{Tong Wei}^{1,2,3} & \textbf{Bo-Lin Wang}^{1,2} & \textbf{Jiang-Xin Shi}^{3,4} \\ & \textbf{Yu-Feng Li}^{3,4} & \textbf{Min-Ling Zhang}^{1,2} \end{array}$

¹School of Computer Science and Engineering, Southeast University, Nanjing, China ²Key Laboratory of Computer Network and Information Integration (Southeast University), Ministry of Education, China

³National Key Laboratory for Novel Software Technology, Nanjing University, China ⁴School of Artificial Intelligence, Nanjing University, China {weit, wangbl}@seu.edu.cn

Abstract

Recognizing out-of-distribution (OOD) samples is essential for deploying robust machine learning systems in open-world environments. While conventional OOD detection approaches rely on feature representations from the penultimate layer of neural networks, they often overlook informative signals embedded in intermediate layers. In this paper, we present a straightforward feature mixing approach for pretrained Transformers, which combines multi-layer representations via calculated importance weights, and identifies OOD samples using Mahalanobis distance in the blended feature space. When in-distribution samples are accessible, we show that parameter-efficient fine-tuning strategies effectively balance classification accuracy and OOD detection performance. We conduct extensive empirical analyses to validate the superiority of our proposed method under zero-shot, and fine-tuning settings using both class-balanced and long-tailed datasets. The source code is available at https://github.com/SEUML/X-Maha.

1 Introduction

In recent years, deep learning models have made significant progress in various domains [40, 24]. However, a critical issue with these models is their tendency to be overly confident in their predictions, even when the input deviates greatly from the data distribution seen during training. This issue underscores the need for effective out-of-distribution (OOD) detection when training deep neural networks (DNNs). The detection of OODs is crucial to ensure the safety of the model in many applications, such as medical diagnostics [43], industrial inspection [3], and autonomous driving [26]. For example, in the field of medical imaging, DNNs may fail to provide an accurate diagnosis when presented with data that falls outside the training data distribution, such as images from an unknown scanner. Therefore, it is imperative for a reliable model not only to recognize in-distribution (ID) samples, but also to flag any OOD input as "unknown".

Existing OOD detection methods design various scoring functions to assign an input sample a likelihood to be OOD, using 1) predicted probabilities [14, 33, 31, 9, 32], 2) output logits [48, 2], and 3) learned features [25, 9, 36] by the model. However, these approaches neglect the rich information in the features learned by the layers of shallow neural networks. Our motivation stems from the observation that while the final features of a neural network are nonlinear transformations of shallow features and inherently retain some information from earlier layers, features extracted from different layers provide diverse representations of the data. Given that certain features may be particularly effective for distinguishing between ID and OOD samples, it is crucial to comprehensively leverage

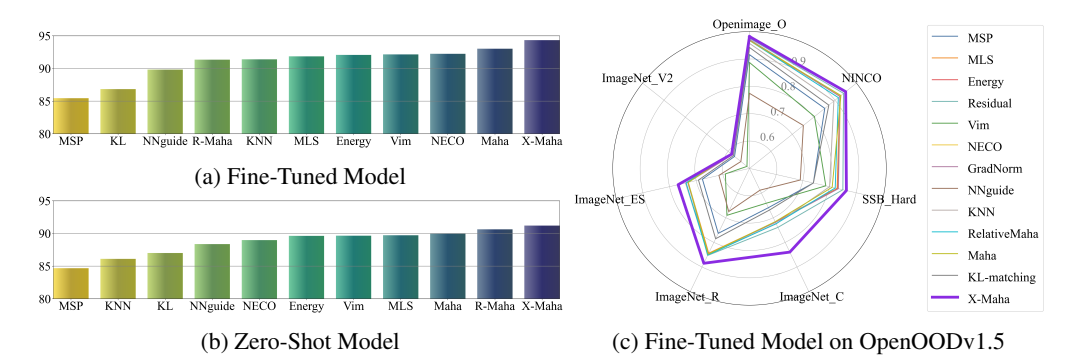


Figure 1: (a-b): AUROC of X-Maha and competing methods based on fine-tuned/zero-shot models. The experimental settings are the same as in Table 2. We denote RelativeMaha as R-Maha. (c) AUROC of X-Maha and competing methods on OpenOODv1.5 benchmark using fine-tuned model.

the information from all layers to enhance OOD detection performance. While the motivation is appealing, a core challenge remains: how to effectively utilize shallow layer features for OOD detection?

To address the above issue, we propose a new OOD detection approach by leveraging features from all layers with an adaptive fusion module. We draw inspiration from the geometric properties of "neural collapse" [37], which states that the convergence of within-class covariance approaches zero in the terminal phase of training as each activation collapses toward its respective class mean. Therefore, we propose to measure the total variance of features across different layers of the neural network to describe their importance weights for OOD detection. Layers with larger total variance have more influence, while the contribution of layers with smaller total variance is down-weighted. The advantage of this method is that layer weights are computed based on the data, without the need for manual parameter tuning. Using the weighted fused features, we calculate the Mahalanobis distance between the test sample and the data distribution of each ID class to calculate its OOD score.

Furthermore, we fine-tune the pre-trained visual models, including Vision Transformer (ViT) [8] and CLIP [39], using in-distribution data to adapt the feature representations to down-stream tasks. We empirically find that parameter-efficient fine-tuning strategies consistently outperforms full parameter fine-tuning and are more robust to hyperparameter choice, which coincides with prior works [44, 11]. Specifically, by freezing the pre-trained model and adding a small number of learnable parameters. Based on this finding, we develop a general fine-tuning framework and implement all comparison methods within this framework in our experiments. We also conducted an in-depth analysis of various fine-tuning strategies. Figure 1 presents the results for in-distribution samples (from ImageNet) processed by ViT-B/16 under various experimental settings. Our X-Maha (X-Mahalanobis) consistently achieves state-of-the-art OOD detection performance in both fine-tuned and zero-shot scenarios, and demonstrates superior performance on the challenging OpenOODv1.5 benchmark.

To systematically evaluate our approach, we focus on both class-balanced ID datasets, which are commonly used in existing OOD detection literature [31, 48, 2], and long-tailed ID datasets because the distribution of real-world data is often imbalanced and highly skewed on a per-class basis, with a majority of classes containing a small number of samples [53, 52, 61]. Notably, long-tailed OOD detection has been studied in several recent works by improving 1) *representation learning* [49, 54, 51, 5], and 2) *probabilistic calibration* [22, 35]. However, these methods often require the use of OOD data to train the model. In contrast, our approach only requires fine-tuning the model using ID data, and more importantly, with no changes needed for the proposed feature mixing module.

Our contributions are summarized as follows:

- 1. We propose a new OOD detection method that exploits features from shallow layers of pre-trained Transformers to enhance OOD separation.
- 2. We propose a simple but effective strategy to fuse multiple layer features with the importance weights by measuring the covariance of features in each layer.

3. We justify the effectiveness of the proposed method in zero-shot setting, and fine-tuning settings using both class-balanced and long-tailed datasets. Additionally, we show that the propose method can generalize to various fine-tuning strategies and pre-trained models.

2 Related Works

Out-of-distribution detection. In recent years, the field of OOD detection has gained considerable attention. The Maximum Softmax Probability (MSP) method [13] serves as a foundational baseline, utilizing softmax predictions as OOD scores. Building on this, ODIN [30] improves the softmax score by perturbing input data and rescaling logits, enhancing its effectiveness in distinguishing OOD samples. Further advancements explore alternative scoring mechanisms, such as the energy score [31], which is further refined through feature clipping in ReAct [45]. Additionally, gradientbased approaches have been explored to differentiate between ID and OOD data [19, 1]. Among previous studies, the use of the Mahalanobis distance has shown significant promise. A prior work [28] proposes to ensemble the Mahalanobis distance score calculated by features of each layer and determine the optimal ensemble weights using an auxiliary OOD validation dataset. Trusted [7] introduces a novel approach that combines feature fusion during training with the Mahalanobis distance during testing, guided by the optimal transport principle. On top of the CLIP model, CLIPN [50] learns a "no" prompt to capture the negation-semantic with images using an auxiliary dataset, and performs OOD detection depending on the similarity between the input image and the "no" prompt. Similarly, NegLabel [23] extracts potential negative labels from a corpus database and employs zero-shot CLIP for OOD detection by combining ID classes and negative labels.

Long-tailed out-of-distribution detection. In long-tailed OOD detection, prior research has examined several strategies to mitigate the challenges posed by class imbalance, including the use of oversampling techniques and threshold adjustments to improve performance [29]. Open Sampling [51] incorporates OOD data to address the class imbalance problem. PASCL [49] focuses on enhancing representation learning for tail classes by leveraging a contrastive learning method, helping to improve the separation between minority classes and OODs. Prior work [22] identifies several common scenarios where the OOD-to-ID probabilities should be the ID-class-prior distribution and proposes two strategies to modify existing inference-time detection methods. EAT [54] proposes expanding the class space of ID classes with virtual classes to tackle OOD data. COCL [35] introduces a calibrated learning approach aimed at improving outlier class detection in long-tailed tasks.

Parameter-efficient fine-tuning. PEFT methods freeze the pre-trained model and introduce only a few learnable parameters for adaptation, which can effectively reduce overfitting and accelerate convergence. Adapter [8] introduces a bottleneck module to optimize only a small subset of parameters. BitFit [58] focuses on fine-tuning only the bias terms of the model, significantly reducing the number of parameters that need to be updated during training. VPT [21] prepends learnable prompts at each layer, offering two versions: VPT-Shallow, which uses prompts at shallow layers, and VPT-Deep, which applies them across deeper layers. LoRA [17] further optimizes efficiency by applying low-rank adaptations, minimizing the overall parameter count while retaining performance. AdaptFormer [4] builds on the Adapter method by shifting from a sequential to a parallel design. LIFT [44] provides an empirical analysis showing that the commonly used full fine-tuning strategy is prone to overfitting, especially on long-tailed datasets.

3 Method

In this section, we present a simple Mahalanobis-based OOD detection method by mixing features from all Transformer layers based on importance weight.

3.1 Preliminary

We first introduce the problem setting and notations used throughout this paper.

1. We denote the training set as $\mathcal{D}_{train} = \{(\boldsymbol{x}_i, y_i)\}_{i=1}^N$, where $\boldsymbol{x}_i \in \mathbb{R}^d$ represents an input image, $y_i \in [C]$ denotes its ground-truth class label, and C denotes the total number of classes in the training set. At test time, our goal is to flag images that do not belong to any of the training classes using our OOD detector.

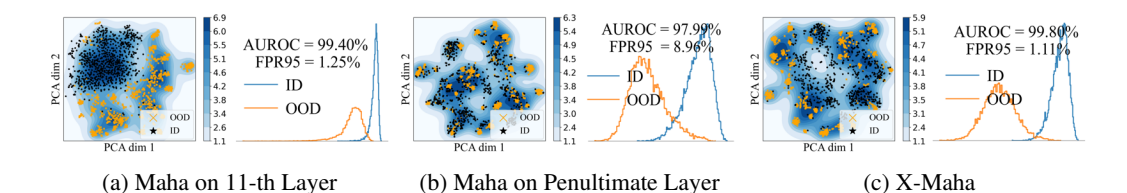


Figure 2: X-Maha: We illustrate how to improve Mahalanobis-based OOD detection. (a) Mahalanobis distance applied to the 11-th layer. (b) Mahalanobis distance applied to the penultimate layer features. (c) X-Maha which is applied to all layer features. Each subfigure comprises two components: a feature visualization map and the corresponding OOD score distribution of test data. The visualizations are based on data sampled from CIFAR-100 (ID) and Tiny ImageNet (OOD) using fine-tuned ViT-B/16.

- 2. Without loss of generality, let the deep neuron network be $F = f \circ g$, where $f(\cdot)$ is known as the feature exactor and $g(\cdot)$ is the classifier. For each layer $\phi(\cdot)$ in f, we define the transformation learned by the l-th layer as $\phi_l(\cdot)$. For an instance x, its output from the l-th layer is denoted as $x^l = \phi_l(x)$. In particular, we denote the final feature learned by the model $x^L = \phi_L(x)$, where L denotes the number of Transformer layers.
- 3. In this paper, we build our OOD detector based on the Mahalanobis distance. For any test image x, we calculate the negative distance between the image feature f(x) and feature distribution of each class as the scoring function:

$$M(\boldsymbol{x}; \boldsymbol{\mu}_c, \boldsymbol{\Sigma}) = -(f(\boldsymbol{x}) - \boldsymbol{\mu}_c)^{\top} \boldsymbol{\Sigma}^{-1} (f(\boldsymbol{x}) - \boldsymbol{\mu}_c),$$
(1)

where μ_c is the mean feature vector of class c and Σ is the covariance matrix of ID data.

4. To measure the Mahalanobis distance, we calculate the empirical class mean and covariance matrix of training samples as follows:

$$\boldsymbol{\mu}_{c} = \frac{1}{N_{c}} \sum_{i: y_{i} = c} f\left(\boldsymbol{x}_{i}\right), \boldsymbol{\Sigma} = \frac{1}{N} \sum_{c=1}^{C} \sum_{i: y_{i} = c} \left(f\left(\boldsymbol{x}_{i}\right) - \boldsymbol{\mu}_{c}\right) \left(f\left(\boldsymbol{x}_{i}\right) - \boldsymbol{\mu}_{c}\right)^{\top},$$
(2)

where N_c is the number of training samples with class c. This is equivalent to fitting the class-conditional Gaussian distribution with a tied covariance to the training samples under the maximum likelihood estimator [28].

3.2 X-Maha: Feature Mixing for Mahalanobis-based OOD Detection

By default, the Mahalanobis distance in Eq. (1) uses the final output of the feature extractor, i.e., f(x), neglecting rich information in shallow layer features. Therefore, we now proceed to present our approach to demonstrate that shallow features can help improve OOD detection performance. For any test image x and a fine-tuned model, we first obtain its hidden representations x_i^l of the l-th layer, $\forall 1 \leq l \leq L$. Notably, we may use "features" and "representations" interchangeably throughout the paper. We then integrate features from all layers by different importance weights. Formally, we compute the fused feature representation of x by:

$$\Phi(\boldsymbol{x}) = \sum_{l=1}^{L} \alpha^l \boldsymbol{x}^l, \tag{3}$$

where α^l is the weight of the l-th layer. To measure the Mahalanobis distance, we also calculate the class mean feature vectors and global covariance matrix in the fused feature space. We reformulate Eq. (2) by fusing shallow features as follows:

$$M_{\text{X-Maha}}(\boldsymbol{x}; \widetilde{\boldsymbol{\mu}}_c, \widetilde{\boldsymbol{\Sigma}}) = -(\Phi(\boldsymbol{x}) - \widetilde{\boldsymbol{\mu}}_c)^{\top} \widetilde{\boldsymbol{\Sigma}}^{-1} (\Phi(\boldsymbol{x}) - \widetilde{\boldsymbol{\mu}}_c), \tag{4}$$

where
$$\widetilde{\boldsymbol{\Sigma}} = \frac{1}{N} \sum_{c=1}^{C} \sum_{i:y_i=c} \left(\Phi(\boldsymbol{x}_i) - \widetilde{\boldsymbol{\mu}}_c \right) \left(\Phi(\boldsymbol{x}_i) - \widetilde{\boldsymbol{\mu}}_c \right)^{\top}$$
 and $\widetilde{\boldsymbol{\mu}}_c = \frac{1}{N_c} \sum_{i:y_i=c} \Phi(\boldsymbol{x}_i)$.

Figure 2 provides an intuitive example in which shallow features can exhibit better discriminativity between ID and OOD data than the final layer features. By mixing features as in Eq. (3), X-Maha can effectively alleviate feature overlapping between ID and OOD data.

We now provide a simple way to set α^l . To reflect the importance of each layer, we propose to calculate the weights by measuring the instance-discrimination capacity or variability of the features.

Definition 3.1 (Measure of Variability). Given a collection of x_l , we calculate the mean feature by $\mu^l = \frac{1}{N} \sum_{i=1}^N x_i^l$, then and measure the feature variability of the l-th layer by:

$$\alpha^l = \text{Tr}((\boldsymbol{A}^l)^\top \boldsymbol{A}^l), \tag{5}$$

where $\mathbf{A}^l = (\mathbf{x}_1^l - \boldsymbol{\mu}^l, \mathbf{x}_2^l - \boldsymbol{\mu}^l, \cdots, \mathbf{x}_N^l - \boldsymbol{\mu}^l)^{\top}$ is the centralized feature matrix of the l-th layer, and $\mathrm{Tr}(\cdot)$ denotes the trace of a matrix, which is the sum of its diagonal elements. We normalize the weights so that the sum of the weights across all layers is equal to 1.

The trace of the matrix $\operatorname{Tr}((A^l)^\top A^l)$ is proportional to the total variance of the features in the l-th layer. A higher value of this trace indicates that the features at this layer are, on average, more spread out across the training samples. This substantial variability suggests that the layer captures diverse and discriminative patterns, making it highly sensitive to differences between instances. Therefore, assigning a higher weight to such layers during feature fusion amplifies the contribution of these more informative representations. Notably, Eq. (5) presents one simple way to set mixing weights, though not necessarily optimal. We leave further optimization for future work, as our focus here is on demonstrating the effectiveness of mixing features from shallow layers.

Distinctions with prior works. Our work differs from *Mahalanobis* [28] and *Trusted* [7], which also use internal representations. 1) *Mahalanobis* calculates the OOD score using the representation of each layer individually and weights them together by training a logistic regression model using the validation set. Our approach computes importance weights from training data and does not require any validation set. 2) *Trusted* treats every layer equally with the same importance and averages the representations. It is clear that certain layer representations may be more effective in detecting OODs, whereas others may bring noise. Our approach can prevent the degradation of the overall OOD detection performance even in the case when the features from some layers are not effective: the weights would be nearly zero for those ineffective layers.

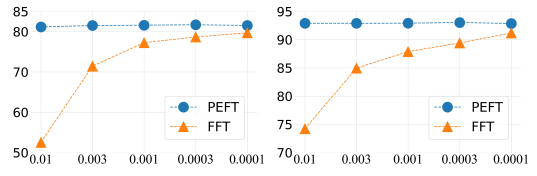
3.3 On the Fine-tuning Strategy for OOD Detection

Parameter-efficient fine-tuning is more robust than fully fine-tuning. To adapt the pre-trained models to downstream classification and OOD detection tasks, we learn a linear classifier and fine-tune the feature extractor using ID training data. In this paper, we adopt the logit adjustment loss [34] as the optimization objective for its simplicity and good generalization ability. The key advantage of this choice is that, for class-balanced ID datasets, it simplifies to the conventional cross-entropy loss; however, for long-tailed ID datasets, it allows the model to balance predictive confidence across classes. Formally, the logit adjustment loss is defined as:

$$\mathcal{L}_{LA}(\boldsymbol{x}, y = j) = -\log \frac{\exp(z_j + \log P(y = j))}{\sum_{k \in [C]} \exp(z_k + \log P(y = k))}$$
(6)

where y = j denotes the ground-truth label of the input x, and z_j is the logit (pre-softmax activation) for class j. The class-prior probability P(y = j) is estimated from the training distribution.

However, when choosing the fine-tuning strategy, we observe that full parameter fine-tuning (FFT) is significantly more sensitive to hyperparameters, such as learning rate, compared to parameter-efficient fine-tuning (PEFT), especially when the ID data follows a long-tailed label distribution. Figure 3 highlights the impact of learning rates on both fine-tuning strategies in CIFAR-100 (ID) classification accuracy and OOD detection AUROC, averaged on six OOD datasets. The *x*-axis denotes the learning rate.



(a) ImageNet-LT ACC (b) ImageNet-LT AUROC

Figure 3: Comparison of the sensitivity of FFT and PEFT to learning rate.

The results indicate that FFT requires careful tuning of learning rates to achieve optimal performance, while PEFT demonstrates more robust performance across a wider range of hyperparameters. Moreover, FFT necessitates tuning hyperparameters like the learning rate individually for each dataset, whereas PEFT allows for consistent hyperparameter settings across multiple datasets, reducing the burden of hyperparameter search.

Extension of our approach to vision-language models. Notably, our proposed X-Maha approach is model-agnostic and can be used for CLIP-like models. Specifically, we calculate the cosine similarity between the image embedding and ID class text prompt embeddings with minimal computational overhead. This similarity score is integrated into X-Maha to improve the effectiveness of OOD detection. Formally, the revised scoring function is defined as follows: $G(x) = \max_{c \in [C]} M_{\text{X-Maha}}(x; \tilde{\mu}_c, \tilde{\Sigma}) + \lambda \cdot \sin(v, t_c)$, where v denotes the image embedding of x extracted by the pre-trained image encoder, and t_c represents the text prompt embedding of class c, i.e., both image and text embeddings are obtained from pre-trained CLIP. The similarity measure $\sin(v, t_c)$ is defined as: $\sin(v, t_c) = \frac{e^{v^\top t_c}}{\sum_k e^{v^\top t_k}}$, where we use the default prompt template "a photo of a {classname}" to obtain text embedding t_c in our experiments. The hyperparameter λ controls the relative influence of the predicted similarity scores of the vision-language model. Notably, we set $\lambda = 0$ when using vision-only models. A test image is classified as OOD if $G(x) \geq \rho$, where ρ is selected such that a high proportion of ID data exceeds this threshold. For samples classified as ID, the class label is determined as $\hat{y} = \arg\max_{c \in [C]} p_c$, where p = F(x) denotes the predicted class probabilities from the classifier.

4 Experiments

We extensively evaluate X-Maha across different datasets and pre-trained models. Due to space constraints, in the main paper, we report the experimental results of models fine-tuned on class-balanced or long-tailed ID datasets.

4.1 Experiments Setup

X-Maha (ours) 99.94

98.13

8.99

In this section, we compare our approach with the latest algorithms across both small- and large-scale OOD detection benchmarks. In line with prior research, we utilize CIFAR-100 and ImageNet as the in-distribution (ID) datasets. Additionally, we incorporate the more challenging long-tailed variants, CIFAR-100-LT and ImageNet-LT, as ID training sets to further demonstrate the effectiveness of our proposed method in OOD detection scenarios in the appendix. The imbalance ratio for CIFAR-100-LT is set to 100, reflecting a highly imbalanced class distribution.

OOD datasets. When CIFAR-100 or CIFAR-100-LT is used as the ID dataset, we evaluate OOD detection performance on a range of diverse datasets, including Textures [6], SVHN [57], CIFAR-10,

Method	Text		SVI			AR10		ageNet	LS		Place		Aver	
Method	AUROC	FPR95	AUROC	FPR95	AUROC	FPR95	AUROC	FPR95	AUROC	FPR95	AUROC	FPR95	AUROC	FPR95
					IMAGEN	ЕТ-21к	PRE-TRA	INED V	ıΤ					
MSP	97.65	11.81	94.91	28.17	94.92	26.32	88.58	44.50	86.75	64.21	92.23	41.41	92.51	36.07
MLS	99.79	0.83	97.38	10.31	97.07	13.42	93.28	25.16	98.09	10.93	98.98	5.39	97.43	11.01
Energy	99.86	0.57	97.48	9.47	97.09	12.88	93.51	23.61	98.59	7.58	99.26	3.78	97.63	9.65
Mahalanobis	99.97	0.12	99.16	3.92	97.09	16.49	97.99	8.96	99.61	1.07	99.67	1.33	98.92	5.32
Residual	99.99	0.02	97.66	12.81	92.08	41.38	99.10	3.68	99.93	0.00	99.92	0.08	98.12	9.66
Vim	99.89	0.44	97.68	8.63	97.13	12.73	94.09	21.96	98.85	5.72	99.39	2.94	97.84	8.74
NECO	99.83	0.83	97.95	8.70	97.31	13.98	94.25	21.93	98.29	10.77	99.08	5.35	97.78	10.26
Trusted	100.0	0.00	98.78	5.77	93.35	33.51	98.09	9.76	100.0	0.01	100.0	0.00	98.37	8.17
KL-matching	98.60	6.10	96.66	14.93	96.34	17.12	90.05	34.17	88.15	49.34	93.67	28.21	93.91	24.98
NNguide	99.24	3.03	98.70	5.00	97.12	17.42	92.48	28.02	93.44	40.52	96.25	21.11	96.21	19.18
RelativeMaha	98.25	6.35	97.44	12.72	96.41	17.73	91.66	34.44	90.66	49.66	94.49	30.37	94.82	25.21
KNN	99.19	3.10	98.51	6.13	96.42	20.66	91.56	30.20	92.79	45.19	96.06	21.73	95.76	21.17
X-Maha (ours)	100.0	0.00	99.50	1.91	96.47	19.52	99.80	1.11	100.0	0.00	100.0	0.00	99.29	3.76
						CLIP-	VIT-B/1	6						
MSP	91.14	41.33	86.22	57.75	87.35	53.18	82.11	62.50	74.83	80.64	84.02	60.61	84.28	59.33
MLS	96.11	20.73	91.58	41.81	93.32	30.69	88.58	45.86	88.49	51.20	93.15	33.12	91.87	37.23
Energy	96.56	18.03	91.85	41.92	93.77	28.89	89.06	44.49	89.66	45.66	93.92	29.21	92.47	34.70
Mahalanobis	99.23	1.68	96.89	23.27	89.01	52.26	93.75	32.28	98.81	6.44	99.29	3.13	96.16	19.84
Residual	99.05	1.86	95.61	31.96	82.22	67.74	94.48	31.92	99.19	3.05	99.36	2.03	94.98	23.09
Vim	97.23	14.33	92.88	36.41	93.82	28.66	89.94	41.40	91.58	38.73	95.13	23.97	93.43	30.58
NECO	97.67	12.20	94.04	33.31	93.57	31.58	90.25	41.08	92.65	34.50	95.90	21.27	94.02	28.99
MCM	72.98	92.09	90.75	63.39	75.53	88.66	65.54	93.36	50.79	99.11	60.97	97.79	69.43	89.06
Trusted	99.98	0.04	97.21	17.80	86.32	61.45	97.13	15.68	99.95	0.03	99.96	0.08	96.76	15.85
KL-matching	94.32	25.12	90.69	38.25	90.69	38.52	84.16	52.94	77.85	70.96	86.99	47.80	87.45	45.60
NNguide	97.91	10.23	97.36	13.61	92.62	17.12	89.88	41.93	86.77	60.83	93.14	35.04	92.95	33.13
RelativeMaha	96.70	14.36	96.44	19.35	91.64	46.09	86.99	51.46	82.57	61.12	91.69	34.71	91.01	37.85
KNN	97.38	13.88	96.93	16.57	91.32	46.27	90.31	39.47	86.24	60.08	93.00	34.22	92.53	35.08

Table 1: OOD detection performance on CIFAR-100 (ID) and six OOD datasets.

97.31

13.23

0.05

0.04

97.33

12.46

52.46

88.74

Tiny ImageNet [27], LSUN [56], and Places365 [60]. For experiments with ImageNet and ImageNet-LT as the ID datasets, our primary evaluation employs five established OOD datasets: Textures [6], Places365 [60], iNaturalist [47], ImageNet-O [15], and SUN [55]. Extended analysis using OpenOODv1.5 [59] is presented in the Appendix.

Baselines. We compare our method with MSP [13], MLS [12], Energy [31], Mahalanobis [28], Residual and Vim [48], NECO [2], MCM [36], Trusted [7], NNguide[38], KNN[46], RelativeMaha[41], and KL-matching [12]. For Mahalanobis, we follow the setting in [10], which uses only the final feature instead of an ensemble of multiple layers [20, 28]. It is worth noting that all these baselines are reimplemented based on our fine-tuned models, except that MCM uses zero-shot CLIP.

Implementation details. We implement our approach and all competing methods in the same framework on top of the ImageNet-21k pre-trained Vision Transformer (ViT) [8] and the official pre-trained CLIP model. We fine-tune the pre-trained models using in-distribution data for downstream tasks. We employ a batch size of 64 for all experiments. For CIFAR-100 and CIFAR-100-LT, we set the initial learning rate to 0.01 with a cosine annealing scheduler and fine-tune for 10 epochs. For ImageNet and ImageNet-LT, the initial learning rate is set to 0.1, with a cosine annealing scheduler, and the models are fine-tuned for 5 and 20 epochs, respectively. We set $\lambda=1$ on ImageNet and $\lambda=0.1$ on CIFAR-100 for the CLIP model to calculate the scoring function. For the Adaptformer module, we set the dimension to $\frac{C}{2L}$, where C is the number of classes, and L is the number of blocks in the ViT model. Other hyperparameters include a momentum of 0.9, and a weight decay of 5×10^{-4} , following LIFT [44]. For all baseline methods, we ensure a fair comparison by using the same hyperparameter settings. All experiments are conducted on a single NVIDIA RTX 3090 GPU.

Table 2: Performance on ImageNet (ID) and five OOD datasets. † indicates the results are taken from their papers, except that results for MCM on ImageNet-O are reproduced using official codebase.

Method	Text		Plac		SU		iNatu		Imagel		Aver	
	AUROC	FPR95	AUROC	FPR95	AUROC	FPR95	AUROC	FPR95	AUROC	FPR95	AUROC	FPR95
]	IMAGEN	ET-21K	PRE-TRA	AINED VI	Т				
MSP	84.89	51.88	84.52	59.44	85.31	56.52	95.86	18.73	82.24	60.00	86.56	49.31
MLS	90.12	37.80	88.01	51.67	89.72	47.21	97.98	8.75	89.79	44.65	91.12	38.02
Energy	90.72	34.65	88.15	50.40	90.06	45.31	98.23	7.41	90.73	41.00	91.58	35.75
Mahalanobis	92.93	26.31	89.27	47.56	91.53	39.82	99.33	2.72	92.12	37.50	93.03	30.78
Residual	92.84	30.66	84.80	61.14	88.34	50.14	98.02	9.51	87.11	52.50	90.22	40.79
Vim	91.04	33.33	88.37	49.82	90.30	44.34	98.37	6.86	90.92	40.20	91.80	34.91
NECO	92.13	30.16	89.92	46.49	91.95	40.11	98.99	4.12	91.45	39.80	92.89	32.14
$NECO^{\dagger}$	92.86	32.44	90.38	42.66	93.15	33.98	99.34	3.26	94.53	25.20	94.05	27.51
Trusted	43.56	86.45	46.82	96.95	50.95	94.75	49.36	91.48	39.15	95.45	45.97	93.02
KL-matching	87.85	40.92	86.76	53.02	87.89	49.19	97.84	8.84	86.25	49.20	89.32	40.23
NNguide	90.98	35.90	87.63	54.90	89.12	51.52	98.62	5.55	90.40	48.00	91.35	39.17
RelativeMaha	90.28	39.80	88.05	52.59	89.83	47.53	99.06	3.54	90.23	46.10	91.49	37.91
KNN	89.18	42.16	85.45	64.49	85.69	66.31	98.03	9.86	87.45	60.45	89.16	48.65
X-Maha (ours)	96.65	11.70	89.64	46.00	92.04	37.78	99.40	2.26	93.76	29.80	94.30	25.51
					CLIP-V	/IT-B/1	6					
MSP	83.05	57.59	79.83	68.39	79.33	70.29	89.74	41.95	78.60	71.00	82.11	61.84
MLS	88.76	45.43	86.02	57.05	86.39	58.28	95.57	23.45	86.53	61.15	88.65	49.07
Energy	89.26	44.01	86.59	54.39	87.12	54.85	96.38	17.67	87.32	58.30	89.33	<u>45.84</u>
Mahalanobis	85.05	66.49	84.34	72.06	85.15	75.37	90.35	65.00	80.71	79.00	85.12	71.58
Residual	76.25	80.05	75.64	88.95	75.40	91.87	71.20	94.15	67.87	88.10	73.27	88.62
Vim	89.30	44.20	86.70	54.49	87.22	55.21	96.17	18.83	87.17	59.25	89.31	46.40
NECO	88.77	47.02	87.86	52.40	88.61	53.92	95.24	25.30	85.29	64.00	89.15	48.53
MCM^{\dagger}	86.11	57.77	89.77	44.69	92.57	37.59	94.61	30.91	79.51	75.70	88.51	49.33
Trusted	95.87	19.80	74.59	78.06	76.71	76.42	84.61	72.77	84.12	62.40	83.18	61.89
KL-matching	86.64	46.45	83.28	59.25	83.21	61.23	94.18	24.99	83.19	62.45	86.10	50.87
NNguide	87.60	51.05	81.94	71.29	82.98	74.77	93.14	38.88	85.27	67.85	86.19	60.77
RelativeMaha	85.14	62.00	81.81	63.13	83.45	63.73	94.53	25.21	83.07	67.75	85.60	56.36
KNN	83.35	68.35	77.31	81.27	76.03	87.32	87.74	75.30	81.63	79.75	81.21	78.40
X-Maha (ours)	89.11	49.52	90.64	41.44	93.11	35.77	95.49	23.04	82.39	69.40	90.15	43.83

4.2 Main Results

Result on CIFAR-100. As shown in Table 1, our proposed method, X-Maha, outperforms state-of-the-art approaches across multiple OOD datasets. In particular, the average performance of X-Maha on both the CLIP model and the ImageNet-21k pre-trained ViT significantly surpasses previous

methods. X-Maha achieves perfect separation of ID and OOD data on Texture, LSUN, and Places 365 datasets. However, we observe a decrease in the performance when using CIFAR-10 as the OOD data. This reduction can be attributed to the high similarity between CIFAR-10 and CIFAR-100 in terms of characteristics, resolution, and visual style—both datasets consist of low-resolution, 32×32 images with somewhat blurred features, making certain samples challenging to differentiate, even for human observers. This resemblance leads to overlapping feature representations in the shallow layers, resulting in relatively diminished performance. Notably, MCM [36] is a zero-shot CLIP-based OOD detection method, and its performance is significantly inferior to other methods, highlighting the necessity of fine-tuning for downstream tasks.

Result on ImageNet. Table 2 summarizes the performance of our proposed method, X-Maha, on the ImageNet dataset. Across both pre-trained models, namely, the ImageNet-21k pre-trained ViT and CLIP-ViT-B/16, X-Maha consistently outperforms existing methods. Specifically, when using the ImageNet-21k pre-trained ViT, X-Maha improves the FPR95 by more than 2% on average compared to the second-best method Mahalanobis [28]. Notably, while MCM [36] does not require fine-tuning, it achieves competitive performance across four OOD datasets, except ImageNet-O. Its overall average performance is on par with the Vim [48] and NECO [2] methods. However, X-Maha still outperforms MCM by $\sim 1.5\%$ in AUROC and $\sim 5.5\%$ in FPR95.

Result on CIFAR-100-LT. Table 3 presents the results on the long-tailed version of CIFAR-100 dataset. It can be seen that our method consistently outperforms previous approaches. When using the CLIP model, our method effectively reduces the FPR95 by an average of 6.31% (from 23.56% to 17.25%).

Table 3: OOD detection performance on CIFAR-100-LT (ID) and six OOD datasets.

Method	Text		SVI		CIFA		Tiny Im		LS		Place		AUDOC	
	AUROC	F1 K33	AUROC				PRE-TRA			F1 K33	AUROC	F1 K33	AUROC	FIKAS
MSP	97.21	13.12	95.52	24.13	91.92	38.50	85.27	48.02	84.06	64.81	90.47	43.10	90.75	38.61
MLS	99.83	0.62	96.38	18.35	94.94	25.58	90.36	34.08	98.58	7.52	99.26	3.06	96.56	14.87
Energy	99.89	0.43	95.65	24.00	94.49	29.42	90.38	34.32	99.09	4.00	99.52	1.62	96.50	15.63
Mahalanobis	99.96	0.43	99.33	2.51	95.09	25.98	97.63	9.26	99.48	2.26	99.57	1.71	98.51	6.99
Residual	99.98	0.20	97.33	17.74	86.41	62.76	98.52	6.90	99.83	0.47	99.80	0.45	96.98	14.73
Vim	99.91	0.03	96.18	20.72	94.56	29.01	91.27	31.59	99.25	3.20	99.60	1.23	96.80	14.73
NECO	99.86	0.64	97.37	13.58	94.91	24.62	91.22	29.21	98.39	10.21	99.22	3.78	96.83	13.67
Trusted	100.0	0.00	99.12	3.60	87.34	52.84	97.67	10.37	99.97	0.00	99.98	0.00	97.35	11.13
KL-matching	98.48	6.40	97.44	12.11	94.00	26.88	87.56	38.91	86.65	52.78	92.94	31.01	92.84	28.02
KL-matching	98.48	6.40	97.44	12.11	94.00	26.88	87.56	38.91	86.65	52.78	92.94	31.01	92.84	28.02
NNguide	99.19	3.30	98.89	3.16	95.10	25.71	90.95	30.58	92.92	34.72	95.60	23.14	95.44	20.10
RelativeMaha	97.25	11.19	96.01	26.31	94.65	26.99	89.94	45.41	90.46	53.53	92.43	38.72	93.46	33.69
KNN	98.82	4.57	97.44	14.68	92.51	36.42	88.45	37.86	89.78	43.25	94.14	28.30	93.52	27.51
X-Maha (ours)	100.0	0.00	99.75	0.43	94.22	29.86	99.75	1.12	99.99	0.00	99.99	0.01	98.95	5.24
						CLIP-	ViT-B/16	5						
MSP	91.05	39.34	86.13	48.73	85.33	55.47	78.22	68.10	73.52	76.50	83.16	57.92	82.90	57.68
MLS	96.76	16.95	88.44	49.78	91.85	36.84	87.05	47.53	90.35	36,77	94.29	25.52	91.46	35.57
Energy	97.31	13.09	86.40	59.64	92.37	34.15	88.01	43.79	92.25	28.45	95.49	19.49	91.97	33.10
Mahalanobis	99.11	1.03	95.92	29.87	84.76	60.58	90.97	43.83	99.08	4.07	99.28	1.99	94.85	23.56
Residual	98.90	1.42	94.83	33.99	77.19	73.51	91.24	48.57	99.28	1.94	99.34	0.87	93.46	26.72
Vim	98.12	9.17	88.61	52.92	92.19	35.68	88.97	41.63	94.26	21.87	96.76	14.76	93.15	29.34
NECO	98.00	9.57	91.32	41.13	91.11	40.21	87.51	46.54	93.99	23.37	96.71	16.22	93.11	29.51
Trusted	99.97	0.11	93.57	43.80	80.76	70.36	95.46	25.58	99.95	0.10	99.95	0.08	94.94	23.34
KL-matching	95.01	21.76	90.76	31.69	88.87	44.17	81.68	57.93	79.31	63.65	87.64	43.21	87.21	43.73
NNguide	96.24	15.50	95.95	20.93	87.06	57.99	84.36	60.30	88.23	48.69	91.11	32.20	90.49	39.27
RelativeMaha	97.25	11.19	96.01	26.31	94.65	26.99	89.94	45.41	90.46	53.53	92.43	38.72	93.46	33.69
KNN	97.48	12.68	91.39	44.15	84.87	59.53	84.54	53.89	83.62	56.77	90.25	41.52	88.69	44.76
X-Maha (ours)	99.90	0.02	97.41	16.80	85.35	59.44	94.85	27.10	99.89	0.10	99.91	0.03	96.22	17.25

Result on ImageNet-LT. Additionally, Table 4 presents the results on the long-tailed ImageNet dataset. It can be seen that our method consistently outperforms previous approaches. On average, our method reduces FPR95 by 5.29% and 2.87% for ImageNet-21k pre-trained ViT and CLIP, respectively. The AUROC also improves by 1.77% when using the CLIP model.

4.3 Ablation Studies

Why X-Maha works? Unless otherwise specified, in this subsection, we use the ImageNet-21k pre-trained ViT as the default base model. Figure 4 presents a comparison of OOD score distributions with and without the application of our proposed X-Maha method. When X-Maha is not applied, only the final layer features are used to compute the Mahalanobis distance as a scoring function.

Table 4: OOD detection performance on ImageNet-LT (ID) and five OOD datasets.

Method	Text		Plac		SU		iNatu AUROC		Imagel		AUROC	
	AUROC	FIROS							AUROC	TIK	AUROC	FIRA
				IMAGEN	ET-ZIK	PRE-TR.	AINED VI	1				
MSP	86.04	47.50	85.20	56.52	86.36	53.07	97.17	11.97	83.68	57.40	87.69	45.29
MLS	90.18	38.71	88.76	49.34	90.39	45.44	98.47	6.71	88.91	47.90	91.34	37.62
Energy	90.87	35.51	89.29	45.97	91.05	41.04	98.78	5.06	89.83	42.80	91.96	34.08
Mahalanobis	92.99	26.95	89.48	46.34	91.71	38.35	99.28	2.84	91.66	38.85	93.02	30.67
Residual	91.60	35.74	82.23	65.71	86.58	55.54	97.44	12.67	84.05	59.05	88.38	45.74
Vim	91.23	34.10	89.47	45.23	91.27	39.83	98.88	4.77	90.05	41.70	92.18	33.13
NECO	91.66	31.44	89.21	43.71	91.44	37.07	98.93	4.09	89.64	42.70	92.18	31.80
Trusted	91.98	32.36	82.11	66.31	85.72	58.34	98.09	9.29	90.91	40.15	89.76	41.29
KL-matching	88.72	38.71	87.41	50.03	89.14	45.83	98.44	6.19	87.24	47.50	90.19	37.65
NNguide	91.06	35.85	87.66	52.60	89.53	48.61	98.66	5.33	90.08	46.55	91.40	37.79
RelativeMaha	89.97	40.74	88.22	52.89	89.92	48.20	98.97	4.01	89.67	47.40	91.35	38.65
KNN	89.80	39.86	85.86	59.61	87.30	56.79	98.21	7.43	87.97	56.10	89.83	43.96
X-Maha (ours)	96.92	11.79	89.82	45.36	92.18	36.16	99.33	2.51	93.46	31.10	94.34	25.38
					CLIP-V	VIT-B/1	6					
MSP	81.55	60.34	79.32	65.16	78.44	66.53	90.60	38.49	78.37	71.60	81.66	60.42
MLS	87.00	52.27	85.31	56.20	85.47	57.19	95.03	25.21	84.33	65.10	87.43	51.19
Energy	87.81	50.07	86.37	51.85	86.76	53.08	95.94	19.61	85.12	63.65	88.40	47.65
Mahalanobis	83.81	67.64	84.44	66.85	85.50	69.58	87.49	72.57	78.82	80.20	84.01	71.37
Residual	74.81	80.71	75.62	86.49	76.56	87.93	63.27	96.67	64.43	89.30	70.94	88.22
Vim	87.90	49.72	86.52	51.32	86.96	52.47	95.55	21.06	84.96	63.90	88.38	47.69
NECO	86.67	53.67	86.71	53.11	87.17	54.63	94.08	29.95	82.90	67.60	87.51	51.79
Trusted	71.96	70.46	44.51	97.89	49.78	97.77	49.44	98.59	48.79	89.05	52.90	90.75
KL-matching	85.35	51.56	82.84	57.00	82.51	57.56	94.54	23.36	82.52	64.00	85.55	50.70
NNguide	86.06	56.44	82.53	65.49	83.68	66.66	90.59	47.29	83.07	71.15	85.18	61.41
RelativeMaha	83.81	67.38	81.84	63.31	82.74	64.13	93.95	31.74	82.25	71.10	84.92	59.53
KNN	82.58	66.42	78.66	74.60	78.64	77.96	83.97	70.68	79.61	79.10	80.69	73.75
X-Maha (ours)	89.94	46.79	90.47	42.51	92.71	37.95	94.79	27.57	82.94	69.10	90.17	44.78

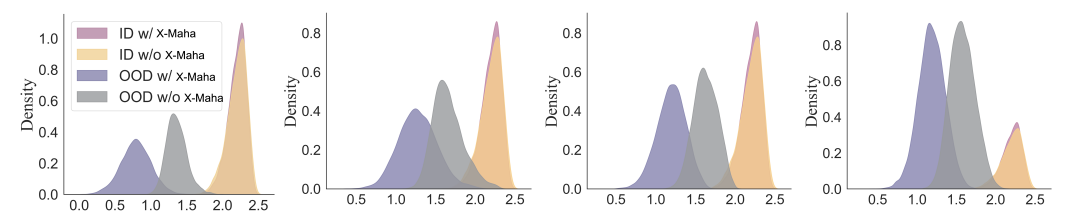


Figure 4: Comparisons of OOD score distribution before and after applying our X-Maha method. CIFAR-100 is used as the ID dataset and the OOD dataset from left to right is Texture, Tiny ImageNet, LSUN, and Places365. The horizontal axis represents the OOD score (small values indicate a high likelihood of being OOD samples).

It can be seen that the score distributions for ID samples remain largely consistent, whether or not the X-Maha method is applied. However, the use of X-Maha causes a significant leftward shift in the score distribution for OOD samples. This shift occurs because the features in the final layer of unseen OOD samples are not effectively captured. Furthermore, re-weighted information from the shallow layers amplifies this shift, resulting in better discrimination. As a result, the X-Maha method enhances the separation between ID and OOD samples in the embedding space. This improvement is critical for more accurate identification and differentiation of ID and OOD samples, thus boosting the overall performance and reliability of the detection process.

Importance weights of each layer. As depicted in Figure 5, our proposed method can adaptively assign importance weights to different layers. Overall, the first 6 layers are assigned relatively lower weights compared to the rest of the Transformer layers. Notably, the final layer's weight is particularly prominent. This is because the last layer of the feature extractor learns the most discriminative features for in-distribution classes and is important for OOD detection. As shown in the figure, rather than relying solely on the penultimate layer's features, our method effectively utilizes shallow layer features as well.

Impact of features from shallow layers. Figure 6 illustrates the effect of fusing features from varying numbers of layers. The x-axis represents the number of layers counted from the penultimate



Figure 5: Distribution of layer-specific weights for CIFAR-100, ImageNet, ImageNet (CLIP), and ImageNet-LT where the y-axis denotes AUROC (%).



Figure 6: Impact of the number of layers used for feature fusion on OOD detection performance. The ID dataset from left to right is CIFAR-100, ImageNet, ImageNet (CLIP), and ImageNet-LT, where the vertical axis represents AUROC.

layer towards the first, while the y-axis indicates the average OOD detection AUROC. As shown in the figures, using only the penultimate layer's features yields decent results, but fusing the last 6 layers of the Transformer achieves the best performance, highlighting the importance of shallow features. For features from the sixth layer and beyond, their impact on the results is minimal. As discussed in the previous analysis, our method assigns lower weights to these layers accordingly.

Table 5: Comparisons of different feature mixing strategies. 'In21k' denotes ViT pre-trained on ImageNet-21k.

		CIFA	R-100			Imag	geNet			
Method	CL	IP	In2	1k	CL	IP	In2	1k	Aver	age
Method	AUROC	FPR95								
Trusted	96.76	15.85	98.37	8.17	83.18	61.89	45.97	93.02	81.49	44.73
SA	96.53	13.19	98.77	6.58	82.68	64.59	94.01	27.62	93.00	28.00
PM	96.15	18.13	98.16	10.05	81.03	77.59	81.86	27.47	89.30	33.31
Flatten12	42.10	89.67	29.00	90.93	-	-	-	-	34.05	90.15
Flatten6	93.31	15.99	81.75	49.33	-	-	-	-	87.53	32.66
Ours	97.33	12.46	99.29	3.76	90.15	43.83	94.30	25.51	95.27	21.39

Ways to fuse shallow features. We compare our proposed feature mixing method with other fusion strategies including 1) Trusted [7] which directly employs the arithmetic mean to fuse features from each layer during both the training and test phases; 2) Score Aggregation (SA) [28] which calculates the OOD score via Mahalanobis distance using features from each layer separately and weighted them together. Since SA requires a validation set containing both ID and OOD data, we use the weights derived from our method to calculate the weighted sum of scores; 3) Power Mean (PM) [42] proposes to reweight each layer's feature based on feature norms; 4) Flatten12 concatenates all layers' features into a single vector, while Flatten6 concatenates the last six layers' features. The results are presented in Table 5. It can be seen that our proposed adaptive fusion method achieves a significant advantage in aggregating shallow features, further confirming its effectiveness.

5 Conclusion

This paper introduces a timely improvement to Mahalanobis-based OOD detection by effectively mixing Transformer features across layers. While shallow features may lack class discrimination, we demonstrate their strength in separating ID and OOD data. Our method assigns importance weights to layer features, without relying on validation data, and leverages parameter-efficient fine-tuning to better adapt pre-trained Transformers for OOD detection. Extensive experiments validate our approach across zero-shot and fine-tuning settings, vision-only and vision-language models, and both balanced and long-tailed ID datasets. Ablation studies further clarify its mechanisms. We believe this work establishes a strong baseline for future OOD detection research.

References

- [1] Chirag Agarwal, Daniel D'souza, and Sara Hooker. Estimating example difficulty using variance of gradients. In *Proceedings of the IEEE/CVF Conference on Computer Vision and Pattern Recognition*, pages 10368–10378, 2022.
- [2] Mouïn Ben Ammar, Nacim Belkhir, Sebastian Popescu, Antoine Manzanera, and Gianni Franchi. NECO: neural collapse based out-of-distribution detection. In *The Twelfth International Conference on Learning Representations*, 2024.
- [3] Paul Bergmann, Michael Fauser, David Sattlegger, and Carsten Steger. Mytec ad–a comprehensive real-world dataset for unsupervised anomaly detection. In *Proceedings of the IEEE/CVF Conference on Computer Vision and Pattern Recognition*, pages 9592–9600, 2019.
- [4] Shoufa Chen, Chongjian Ge, Zhan Tong, Jiangliu Wang, Yibing Song, Jue Wang, and Ping Luo. Adapt-former: Adapting vision transformers for scalable visual recognition. Advances in Neural Information Processing Systems, 35:16664–16678, 2022.
- [5] Hyunjun Choi, JaeHo Chung, Hawook Jeong, and Jin Young Choi. Three factors to improve out-of-distribution detection. *arXiv* preprint arXiv:2308.01030, 2023.
- [6] Mircea Cimpoi, Subhransu Maji, Iasonas Kokkinos, Sammy Mohamed, and Andrea Vedaldi. Describing textures in the wild. In *Proceedings of the IEEE Conference on Computer Vision and Pattern Recognition*, pages 3606–3613, 2014.
- [7] Pierre Colombo, Eduardo DC Gomes, Guillaume Staerman, Nathan Noiry, and Pablo Piantanida. Beyond mahalanobis-based scores for textual ood detection. *arXiv preprint arXiv:2211.13527*, 2022.
- [8] Alexey Dosovitskiy, Lucas Beyer, Alexander Kolesnikov, Dirk Weissenborn, Xiaohua Zhai, Thomas Unterthiner, Mostafa Dehghani, Matthias Minderer, Georg Heigold, Sylvain Gelly, et al. An image is worth 16x16 words: Transformers for image recognition at scale. *arXiv preprint arXiv:2010.11929*, 2020.
- [9] Stanislav Fort, Jie Ren, and Balaji Lakshminarayanan. Exploring the limits of out-of-distribution detection. In *Advances in Neural Information Processing Systems 34*, pages 7068–7081, 2021.
- [10] Stanislav Fort, Jie Ren, and Balaji Lakshminarayanan. Exploring the limits of out-of-distribution detection. Advances in Neural Information Processing Systems, 34:7068–7081, 2021.
- [11] Kai Gan and Tong Wei. Erasing the bias: Fine-tuning foundation models for semi-supervised learning. In *Proceedings of the 41st International Conference on Machine Learning*, pages 14453–14470, 2024.
- [12] Dan Hendrycks, Steven Basart, Mantas Mazeika, Andy Zou, Joe Kwon, Mohammadreza Mostajabi, Jacob Steinhardt, and Dawn Song. Scaling out-of-distribution detection for real-world settings. *arXiv preprint arXiv:1911.11132*, 2019.
- [13] Dan Hendrycks and Kevin Gimpel. A baseline for detecting misclassified and out-of-distribution examples in neural networks. *arXiv preprint arXiv:1610.02136*, 2016.
- [14] Dan Hendrycks, Mantas Mazeika, and Thomas Dietterich. Deep anomaly detection with outlier exposure. In ICLR, 2019.
- [15] Dan Hendrycks, Kevin Zhao, Steven Basart, Jacob Steinhardt, and Dawn Song. Natural adversarial examples. In *Proceedings of the IEEE/CVF Conference on Computer Vision and Pattern Recognition*, pages 15262–15271, 2021.
- [16] Neil Houlsby, Andrei Giurgiu, Stanislaw Jastrzebski, Bruna Morrone, Quentin De Laroussilhe, Andrea Gesmundo, Mona Attariyan, and Sylvain Gelly. Parameter-efficient transfer learning for NLP. In Proceedings of the 36th International Conference on Machine Learning, pages 2790–2799, 2019.
- [17] Edward J Hu. yelong shen, phillip wallis, zeyuan allen-zhu, yuanzhi li, shean wang, lu wang, and weizhu chen. lora: Low-rank adaptation of large language models. In *International Conference on Learning Representations*, volume 3, page 7, 2022.
- [18] Edward J Hu, yelong shen, Phillip Wallis, Zeyuan Allen-Zhu, Yuanzhi Li, Shean Wang, Lu Wang, and Weizhu Chen. LoRA: Low-rank adaptation of large language models. In *International Conference on Learning Representations*, 2022.
- [19] Rui Huang, Andrew Geng, and Yixuan Li. On the importance of gradients for detecting distributional shifts in the wild. Advances in Neural Information Processing Systems, 34:677–689, 2021.

- [20] Rui Huang and Yixuan Li. Mos: Towards scaling out-of-distribution detection for large semantic space. In Proceedings of the IEEE/CVF Conference on Computer Vision and Pattern Recognition, pages 8710–8719, 2021.
- [21] Menglin Jia, Luming Tang, Bor-Chun Chen, Claire Cardie, Serge Belongie, Bharath Hariharan, and Ser-Nam Lim. Visual prompt tuning. In European Conference on Computer Vision, pages 709–727, 2022.
- [22] Xue Jiang, Feng Liu, Zhen Fang, Hong Chen, Tongliang Liu, Feng Zheng, and Bo Han. Detecting out-of-distribution data through in-distribution class prior. In *International Conference on Machine Learning*, pages 15067–15088, 2023.
- [23] Xue Jiang, Feng Liu, Zhen Fang, Hong Chen, Tongliang Liu, Feng Zheng, and Bo Han. Negative label guided ood detection with pretrained vision-language models. In *International Conference on Learning Representations (ICLR)*, 2024.
- [24] John Jumper, Richard Evans, Alexander Pritzel, Tim Green, Michael Figurnov, Olaf Ronneberger, Kathryn Tunyasuvunakool, Russ Bates, Augustin Žídek, Anna Potapenko, et al. Highly accurate protein structure prediction with alphafold. *Nature*, 596(7873):583–589, 2021.
- [25] Ryo Kamoi and Kei Kobayashi. Why is the mahalanobis distance effective for anomaly detection? *arXiv* preprint arXiv:2003.00402, 2020.
- [26] Bernd Kitt, Andreas Geiger, and Henning Lategahn. Visual odometry based on stereo image sequences with ransac-based outlier rejection scheme. In IEEE Intelligent Vehicles Symposium, pages 486–492, 2010.
- [27] Ya Le and Xuan Yang. Tiny imagenet visual recognition challenge. CS 231N, 7(7):3, 2015.
- [28] Kimin Lee, Kibok Lee, Honglak Lee, and Jinwoo Shin. A simple unified framework for detecting out-of-distribution samples and adversarial attacks. Advances in Neural Information Processing Systems, 31, 2018.
- [29] Bolian Li, Zongbo Han, Haining Li, Huazhu Fu, and Changqing Zhang. Trustworthy long-tailed classification. In Proceedings of the IEEE/CVF Conference on Computer Vision and Pattern Recognition, pages 6970–6979, 2022.
- [30] Shiyu Liang, Yixuan Li, and Rayadurgam Srikant. Enhancing the reliability of out-of-distribution image detection in neural networks. arXiv preprint arXiv:1706.02690, 2017.
- [31] Weitang Liu, Xiaoyun Wang, John Owens, and Yixuan Li. Energy-based out-of-distribution detection. Advances in neural information processing systems, 33:21464–21475, 2020.
- [32] Xixi Liu, Yaroslava Lochman, and Christopher Zach. Gen: Pushing the limits of softmax-based out-ofdistribution detection. In *Proceedings of the IEEE/CVF Conference on Computer Vision and Pattern Recognition*, pages 23946–23955, 2023.
- [33] Alexander Meinke and Matthias Hein. Towards neural networks that provably know when they don't know. In *ICLR*, 2020.
- [34] Aditya Krishna Menon, Sadeep Jayasumana, Ankit Singh Rawat, Himanshu Jain, Andreas Veit, and Sanjiv Kumar. Long-tail learning via logit adjustment. *arXiv preprint arXiv:2007.07314*, 2020.
- [35] Wenjun Miao, Guansong Pang, Xiao Bai, Tianqi Li, and Jin Zheng. Out-of-distribution detection in long-tailed recognition with calibrated outlier class learning. In *Proceedings of the AAAI Conference on Artificial Intelligence*, pages 4216–4224, 2024.
- [36] Yifei Ming, Ziyang Cai, Jiuxiang Gu, Yiyou Sun, Wei Li, and Yixuan Li. Delving into out-of-distribution detection with vision-language representations. In Advances in Neural Information Processing Systems, 2022.
- [37] Vardan Papyan, XY Han, and David L Donoho. Prevalence of neural collapse during the terminal phase of deep learning training. Proceedings of the National Academy of Sciences, 117(40):24652–24663, 2020.
- [38] Jaewoo Park, Yoon Gyo Jung, and Andrew Beng Jin Teoh. Nearest neighbor guidance for out-of-distribution detection. In Proceedings of the IEEE/CVF international conference on computer vision, pages 1686–1695, 2023.
- [39] Alec Radford, Jong Wook Kim, Chris Hallacy, Aditya Ramesh, Gabriel Goh, Sandhini Agarwal, Girish Sastry, Amanda Askell, Pamela Mishkin, Jack Clark, et al. Learning transferable visual models from natural language supervision. In *International Conference on Machine Learning*, pages 8748–8763, 2021.

- [40] Aditya Ramesh, Mikhail Pavlov, Gabriel Goh, Scott Gray, Chelsea Voss, Alec Radford, Mark Chen, and Ilya Sutskever. Zero-shot text-to-image generation. In *International Conference on Machine Learning*, pages 8821–8831, 2021.
- [41] Jie Ren, Stanislav Fort, Jeremiah Liu, Abhijit Guha Roy, Shreyas Padhy, and Balaji Lakshminarayanan. A simple fix to mahalanobis distance for improving near-ood detection. arXiv preprint arXiv:2106.09022, 2021.
- [42] Andreas Rücklé, Steffen Eger, Maxime Peyrard, and Iryna Gurevych. Concatenated power mean word embeddings as universal cross-lingual sentence representations. arXiv preprint arXiv:1803.01400, 2018.
- [43] Thomas Schlegl, Philipp Seeböck, Sebastian M Waldstein, Ursula Schmidt-Erfurth, and Georg Langs. Unsupervised anomaly detection with generative adversarial networks to guide marker discovery. In *International Conference on Information Processing in Medical Imaging*, pages 146–157, 2017.
- [44] Jiang-Xin Shi, Tong Wei, Zhi Zhou, Jie-Jing Shao, Xin-Yan Han, and Yu-Feng Li. Long-tail learning with foundation model: Heavy fine-tuning hurts. In Forty-first International Conference on Machine Learning, 2024.
- [45] Yiyou Sun, Chuan Guo, and Yixuan Li. React: Out-of-distribution detection with rectified activations. *Advances in Neural Information Processing Systems*, 34:144–157, 2021.
- [46] Yiyou Sun, Yifei Ming, Xiaojin Zhu, and Yixuan Li. Out-of-distribution detection with deep nearest neighbors. In *International Conference on Machine Learning*, pages 20827–20840, 2022.
- [47] Grant Van Horn, Oisin Mac Aodha, Yang Song, Yin Cui, Chen Sun, Alex Shepard, Hartwig Adam, Pietro Perona, and Serge Belongie. The inaturalist species classification and detection dataset. In *Proceedings of the IEEE Conference on Computer Vision and Pattern Recognition*, pages 8769–8778, 2018.
- [48] Haoqi Wang, Zhizhong Li, Litong Feng, and Wayne Zhang. Vim: Out-of-distribution with virtual-logit matching. In *Proceedings of the IEEE/CVF conference on computer vision and pattern recognition*, pages 4921–4930, 2022.
- [49] Haotao Wang, Aston Zhang, Yi Zhu, Shuai Zheng, Mu Li, Alex J Smola, and Zhangyang Wang. Partial and asymmetric contrastive learning for out-of-distribution detection in long-tailed recognition. In *International Conference on Machine Learning*, pages 23446–23458, 2022.
- [50] Hualiang Wang, Yi Li, Huifeng Yao, and Xiaomeng Li. Clipn for zero-shot ood detection: Teaching clip to say no. In Proceedings of the IEEE/CVF International Conference on Computer Vision, pages 1802–1812, 2023.
- [51] Hongxin Wei, Lue Tao, Renchunzi Xie, Lei Feng, and Bo An. Open-sampling: Exploring out-ofdistribution data for re-balancing long-tailed datasets. In *International Conference on Machine Learning*, pages 23615–23630, 2022.
- [52] Tong Wei and Kai Gan. Towards realistic long-tailed semi-supervised learning: Consistency is all you need. In *IEEE/CVF Conference on Computer Vision and Pattern Recognition*, pages 3469–3478, 2023.
- [53] Tong Wei, Zhen Mao, Zi-Hao Zhou, Yuanyu Wan, and Min-Ling Zhang. Learning label shift correction for test-agnostic long-tailed recognition. In *Proceedings of the 41st International Conference on Machine Learning*, pages 52611–52631, 2024.
- [54] Tong Wei, Bo-Lin Wang, and Min-Ling Zhang. Eat: Towards long-tailed out-of-distribution detection. In Proceedings of the AAAI Conference on Artificial Intelligence, pages 15787–15795, 2024.
- [55] Jianxiong Xiao, James Hays, Krista A Ehinger, Aude Oliva, and Antonio Torralba. Sun database: Large-scale scene recognition from abbey to zoo. In 2010 IEEE Computer Society Conference on Computer Vision and Pattern Recognition, pages 3485–3492, 2010.
- [56] Fisher Yu, Yinda Zhang, Shuran Song, Ari Seff, and Jianxiong Xiao. Lsun: Construction of a large-scale image dataset using deep learning with humans in the loop. *Computer Science*, 2015.
- [57] Netzer Yuval. Reading digits in natural images with unsupervised feature learning. In *Proceedings of the NIPS Workshop on Deep Learning and Unsupervised Feature Learning*, 2011.
- [58] Elad Ben Zaken, Shauli Ravfogel, and Yoav Goldberg. Bitfit: Simple parameter-efficient fine-tuning for transformer-based masked language-models. arXiv preprint arXiv:2106.10199, 2021.

- [59] Jingyang Zhang, Jingkang Yang, Pengyun Wang, Haoqi Wang, Yueqian Lin, Haoran Zhang, Yiyou Sun, Xuefeng Du, Yixuan Li, Ziwei Liu, Yiran Chen, and Hai Li. Openood v1.5: Enhanced benchmark for out-of-distribution detection. *arXiv* preprint arXiv:2306.09301, 2023.
- [60] Bolei Zhou, Aditya Khosla, Agata Lapedriza, Antonio Torralba, and Aude Oliva. Places: An image database for deep scene understanding. *arXiv preprint arXiv:1610.02055*, 2016.
- [61] Zi-Hao Zhou, Siyuan Fang, Zi-Jing Zhou, Tong Wei, Yuanyu Wan, and Min-Ling Zhang. Continuous contrastive learning for long-tailed semi-supervised recognition. In *Advances in Neural Information Processing Systems 38*, pages 51411–51435, 2024.

A Additional Experiments

A.1 Zero-shot OOD detection performance

To further demonstrate the effectiveness of our proposed feature mixing approach, we evaluate the zero-shot performance without fine-tuning pre-trained models using ID datasets. The results are reported in Table 6.

Table 6: OOD detection performance on ImageNet-LT (ID) and five OOD datasets using the pre-trained models without fine-tuning.

Method	Text AUROC		Plac AUROC		SU AUROC		iNatu AUROC		Imagel AUROC		Aver AUROC	
]	IMAGEN	Тет-21к I	PRE-TRA	AINED VI	T				
MSP	84.92	50.12	81.63	68.06	81.77	68.88	95.02	24.12	80.04	64.65	84.68	55.17
MLS	91.01	36.22	84.48	61.71	86.96	56.93	96.88	17.52	89.31	52.45	89.73	44.97
Energy	91.17	36.44	84.11	62.57	86.91	56.66	96.30	22.56	89.72	51.90	89.64	46.03
Mahalanobis	93.13	24.63	81.79	67.52	85.16	61.30	98.63	5.59	91.26	41.30	89.99	40.07
Residual	91.78	33.83	64.01	86.88	71.16	80.23	94.44	27.58	83.22	58.95	80.92	57.49
Vim	91.51	34.47	83.98	62.44	86.90	56.37	96.57	20.37	89.94	50.15	89.78	44.76
NECO	92.54	27.00	79.76	65.31	83.77	60.32	98.55	5.37	90.27	43.50	88.98	40.30
KL-matching	87.51	40.66	83.23	64.05	84.18	61.98	96.72	16.12	83.40	55.15	87.01	47.59
X-Maha (ours)	97.15	10.20	81.51	67.20	85.49	56.49	98.69	5.13	93.15	32.15	91.20	34.23
					CLIP-V	/IT-B/1	6					
MSP	76.67	82.07	61.22	94.21	61.62	96.00	72.78	92.94	70.56	89.95	68.57	91.03
MLS	76.88	91.90	78.12	85.99	76.29	93.61	74.86	95.57	74.28	89.20	76.09	91.25
Energy	69.74	97.02	78.19	89.82	75.68	96.23	69.13	98.24	69.40	92.55	72.43	94.77
Mahalanobis	69.91	94.86	70.20	96.58	67.53	98.78	67.77	98.96	70.57	90.30	69.20	95.90
Residual	64.57	96.51	59.59	98.11	55.23	99.38	49.12	99.35	62.89	91.65	58.28	97.00
Vim	69.34	96.99	76.89	91.80	74.19	97.36	67.49	98.44	68.96	92.10	71.37	95.34
NECO	73.70	92.59	73.55	93.38	71.99	97.32	70.80	98.68	70.96	89.65	72.20	94.32
KL-matching	83.71	63.99	62.27	86.25	63.80	88.92	79.40	79.31	74.73	80.90	72.78	<u>79.87</u>
X-Maha (ours)	87.74	58.03	88.22	59.63	89.77	61.21	91.07	55.93	80.75	76.60	87.51	62.28

A.2 In-distribution classification accuracy

Our fine-tuned model also shows strong ID classification performance, as detailed in Table 7. In terms of overall accuracy, both CIFAR-100 and ImageNet-1k perform better with balanced data compared to long-tailed data. This indicates that data balance positively impacts model performance, facilitating more accurate classification tasks.

When comparing different models, the pre-trained ViT consistently outperform CLIP-ViT-B/16 in most scenarios. This indicates that the pre-trained ViT has specific advantages for these data sets and tasks, suggesting that its pre-training approach is more suitable for these classification tasks, thereby also enhancing its efficacy in OOD detection tasks.

A.3 Ablation studies on weights of different layers

To further emphasize the importance of differentiated layer weighting, we provide experimental tables (i.e., Table 8, 9, 10). In these Tables, we test different scenarios where the final layer is given weights of 0.083 (i.e., uniform), 0.5, 0.75, and 1 (which are represented by $W_{0.083}, W_{0.5}, W_{0.75}, W_{1.0}$), while the other layers receive the remaining weights evenly. Overall, the OOD detection performance

Table 7: Top 1% accuracy on ID data for the original classification task, for the models.

ID dataset	Label distribution	Model	Accuracy (%)
	Zero-shot	CLIP-ViT-B/16	66.69
		CLIP-ViT-B/16	82.87
CIFAR-100	Long-tailed	Pre-trained ViT	89.99
		CLIP-ViT-B/16	88.59
	Balanced	Pre-trained ViT	93.47
	Zero-shot	CLIP-ViT-B/16	67.12
		CLIP-ViT-B/16	75.82
ImageNet-1k	Long-tailed	Pre-trained ViT	81.79
		CLIP-ViT-B/16	79.08
	Balanced	Pre-trained ViT	83.50

Table 8: Ablation studies on weights of different layers on CIFAR-100 (ID).

Method	Text AUROC		SVI AUROC		CIFA AUROC		Tiny Im AUROC		LSU AUROC		Place AUROC		Aver AUROC	
					IMAGEN	ет-21к	PRE-TRA	INED V	ıΤ					
$W_{0.083}$	100.0	0.00	99.61	0.28	90.02	51.14	100.0	0.00	100.0	0.00	100.0	0.00	98.27	8.57
$W_{0.5}$	100.0	0.00	99.43	2.36	96.76	18.26	99.62	1.81	100.0	0.00	99.99	0.01	99.30	3.74
$W_{0.75}$	99.99	0.04	99.27	3.33	96.99	16.82	98.83	5.22	99.89	0.06	99.89	0.26	99.14	4.29
$W_{1.0}$	99.97	0.12	99.16	3.92	97.09	16.49	97.99	8.96	99.61	1.07	99.67	1.33	98.92	5.32
X-Maha (ours)	100.0	0.00	99.50	1.91	96.47	19.52	99.80	1.11	100.0	0.00	100.0	0.00	99.29	<u>3.76</u>
						CLIP-	VIT-B/10	5						
$W_{0.083}$	100.0	0.00	99.05	2.82	83.92	65.74	99.94	0.08	100.0	0.00	100.0	0.00	97.15	11.44
$W_{0.5}$	99.92	0.07	98.00	10.27	89.15	51.09	96.49	17.36	99.88	0.21	99.91	0.12	97.22	13.19
$W_{0.75}$	99.61	0.85	97.84	12.34	89.36	50.66	94.38	26.56	99.24	3.85	99.55	1.68	96.66	15.99
$W_{1.0}$	99.23	1.68	96.89	23.27	89.01	52.26	93.75	32.28	98.81	6.44	99.29	3.13	96.16	19.84
X-Maha (ours)	99.95	0.02	98.31	8.62	88.56	53.97	97.54	12.91	99.93	0.06	99.95	0.02	97.37	12.60

is sensitive to layer weights; however, our X-Maha approach consistently achieves remarkable performance.

Table 9: Ablation studies on weights of different layers on CIFAR-100-LT (ID).

					•				•			•		
Method	Text AUROC		SVI AUROC		CIFA AUROC		Tiny Im		LSU AUROC		Place AUROC		Aver AUROC	
					IMAGEN	ет-21к	PRE-TRA	INED V	ΙΤ					
$W_{0.083}$	100.0	0.00	99.85	0.01	85.54	68.56	100.0	0.00	100.0	0.00	100.0	0.00	97.57	11.43
$W_{0.5}$	100.0	0.00	99.68	0.68	94.56	27.90	99.58	1.68	99.99	0.00	99.98	0.01	98.97	5.05
$W_{0.75}$	99.99	0.05	99.49	1.66	94.93	26.42	98.67	5.57	99.81	0.39	99.83	0.53	98.79	5.77
$W_{1,0}$	99.96	0.20	99.33	2.51	95.09	25.98	97.63	9.26	99.48	2.26	99.57	1.71	98.51	6.99
X-Maha (ours)	100.0	0.00	99.75	0.43	94.22	29.86	99.75	1.12	99.99	0.00	99.99	0.01	98.95	<u>5.24</u>
						CLIP-	VIT-B/1	6						
$W_{0.083}$	100.0	0.00	98.76	5.09	80.77	68.39	99.89	0.20	100.0	0.00	100.0	0.00	96.57	12.28
$W_{0.5}$	99.88	0.04	97.37	16.90	85.52	58.97	94.36	28.65	99.87	0.11	99.89	0.05	96.15	17.45
$W_{0.75}$	99.52	0.55	97.15	19.66	85.73	58.99	91.58	39.22	99.36	2.63	99.52	1.20	95.48	20.38
$W_{1.0}$	99.11	1.03	95.92	29.87	84.76	60.58	90.97	43.83	99.08	4.07	99.28	1.99	94.85	23.50
X-Maha (ours)	99.94	0.00	98.13	8.99	88.74	52.46	97.31	13.23	99.93	0.05	99.95	0.04	97.33	12.46

A.4 Ablation studies on smaller pre-trained transformers

As depicted in Table 11, 12, 13, and 14, we have included models like vit_tiny_patch16_224 and vit_small_patch16_224, shown in the upper and lower sections of each table. The outcomes from these smaller models provide further confirmation that our OOD score remains robust and effective across various model scales, thereby enhancing the generalizability and reliability of our proposed approach.

Table 10: Ablation studies on weights of different layers on ImageNet-1k-LT (ID).

Method	Text AUROC		Plac AUROC		SU AUROC		iNatu AUROC		Image AUROC		Aver AUROC	
]	IMAGEN	ЕТ-21к	PRE-TRA	AINED V	ıΤ				
$W_{0.083}$	98.55	6.45	86.32	60.57	88.92	49.25	98.02	9.42	91.72	37.05	92.71	32.55
$W_{0.5}$	95.02	17.96	89.76	44.79	92.08	36.60	99.36	2.63	92.68	34.30	93.78	27.26
$W_{0.75}$	93.78	23.39	89.62	45.54	91.88	37.22	99.32	2.74	92.06	36.75	93.33	29.13
$W_{1.0}$	92.99	26.95	89.48	46.34	91.71	38.35	99.28	2.84	91.66	38.85	93.02	30.67
X-Maha (ours)	96.92	11.79	89.82	45.36	92.18	36.16	99.33	2.51	93.46	31.10	94.34	25.38
					CLIP-	VIT-B/1	6					
$W_{0.083}$	92.23	36.76	91.11	39.65	93.02	36.38	94.62	29.54	83.30	67.45	90.86	41.96
$W_{0.5}$	88.52	52.23	89.87	45.47	92.21	40.58	94.54	28.45	82.56	71.00	89.54	47.55
$W_{0.75}$	87.68	55.39	89.69	46.37	92.08	41.23	94.41	29.30	82.23	72.40	89.22	48.94
$W_{1.0}$	83.81	67.64	84.44	66.85	85.50	69.58	87.49	72.57	78.82	80.20	84.01	71.37
X-Maha (ours)	89.94	46.79	90.47	42.51	92.71	37.95	94.79	27.57	82.94	69.10	90.17	<u>44.78</u>

Table 11: OOD detection performance on CIFAR-100 (ID) on smaller transformers.

Method	Text	ure	SVI	HN	CIFA	R10	Tiny Im	ageNet	LSU	JN	Place	s365	Aver	age
Method	AUROC	FPR95	AUROC	FPR95	AUROC	FPR95	AUROC	FPR95	AUROC	FPR95	AUROC	FPR95	AUROC	FPR95
					VIT	_TINY_	РАТСН16	_224						
MSP	92.09	35.34	83.28	61.28	83.30	63.73	79.89	69.73	72.86	84.07	82.13	65.55	82.26	63.28
MLS	98.62	6.13	92.09	35.85	87.39	54.92	87.71	52.79	88.92	57.57	94.27	30.32	91.50	39.60
Energy	99.03	4.26	92.78	32.41	87.28	55.96	88.18	51.27	90.32	51.04	95.25	24.94	92.14	36.65
Mahalanobis	99.90	0.35	96.28	15.78	87.78	56.67	92.48	33.81	98.20	9.10	98.77	6.27	95.57	20.33
Residual	99.71	0.85	86.24	52.70	76.86	72.72	90.89	42.55	97.46	14.02	97.25	13.66	91.40	32.75
Vim	99.19	3.62	92.99	31.18	87.49	54.90	88.70	48.96	91.14	47.63	95.67	22.63	92.53	34.82
NECO	99.17	3.83	92.34	34.24	87.85	53.47	89.47	46.45	92.38	43.05	96.06	21.11	92.88	33.69
KL-matching	95.41	18.40	87.58	45.71	86.32	53.75	82.47	60.45	75.28	79.24	85.65	52.82	85.45	51.73
X-Maha (ours)	100.0	0.02	96.85	14.13	86.48	60.56	97.00	15.34	99.98	0.01	99.96	0.10	96.71	15.03
					VIT_	SMALL_	РАТСН1	6_224						
MSP	95.98	19.17	92.29	38.18	90.82	39.01	85.95	52.36	82.84	68.92	89.31	47.87	89.53	44.25
MLS	99.28	3.16	96.35	18.16	95.22	24.90	92.18	32.72	96.21	25.40	97.71	13.44	96.16	19.63
Energy	99.48	2.29	96.54	16.55	95.42	23.24	92.59	29.99	97.12	18.57	98.25	10.09	96.57	16.79
Mahalanobis	99.91	0.59	99.05	4.72	94.65	28.65	97.53	11.36	99.60	1.78	99.54	2.52	98.38	8.27
Residual	99.96	0.11	98.60	7.06	88.66	52.27	98.09	9.68	99.65	0.75	99.67	1.14	97.44	11.83
Vim	99.56	1.99	96.88	14.63	95.46	23.06	93.17	27.68	97.52	16.28	98.47	8.82	96.84	15.41
NECO	99.50	2.16	96.76	15.91	95.33	24.33	93.49	26.62	97.26	17.04	98.29	9.75	96.77	15.97
KL-matching	97.66	9.24	94.75	22.21	93.18	28.02	88.04	40.26	85.27	55.47	91.73	33.41	91.77	31.43
X-Maha (ours)	100.0	0.00	99.36	3.16	94.09	31.35	99.47	2.69	99.99	0.01	99.99	0.01	98.82	6.20

A.5 Additional time consumption analysis

Unlike the direct Mahalanobis distance, which considers only the final layer of features, our approach necessitates the integration of features across all layers. This inevitably leads to additional time consumption. Table 15 presents the time consumption at different stages of the test phase, measured in seconds, on the ImageNet-LT dataset (ID) and the fine-tuned ViT model. "Pre-process" represents the process of pre-processing the ID training set, including the calculation of the mean and covariance matrix required for Mahalanobis distance, with additional importance weights α for X-Maha. Each subsequent column represents the time required to process each dataset including the ID test set and OOD datasets, and the last column represents the total time consumed. From the results, we observe that our approach only brings about an additional 10% total time consumption, but results in an improvement of AUROC by 2.39% and a reduction of FPR95 by 7.66% on average, demonstrating the efficacy of our approach.

A.6 Fair comparison with MCM

The MCM method is naturally better suited for zero-shot OOD tasks compared to fine-tuning tasks. The prevalent fine-tuning approach, which mainly targets the visual encoder, tends to disrupt the initial alignment between the visual and text components after fine-tuning, resulting in less effective outcomes. Our goal in including the MCM method in our experiment was not to make a direct comparison but to empirically showcase that our proposed method enhances OOD detection performance. Conversely, methods like ViM and NECO are methodologically and conceptually more similar to our approach and, therefore, require a more thorough comparison. Moreover, we present the results of MCM on the fine-tuned model (i.e., MCM-tuned) in Table 16 for comparison.

Table 12: OOD detection performance on CIFAR-100-LT (ID) on smaller transformers.

Method	Text	ure	SVI	HN	CIFA	R10	Tiny Im	ageNet	LSU	JN	Place	s365	Aver	age
Method	AUROC	FPR95	AUROC	FPR95	AUROC	FPR95	AUROC	FPR95	AUROC	FPR95	AUROC	FPR95	AUROC	FPR95
					VIT	_TINY_	РАТСН16	_224						
MSP	90.08	43.37	81.70	67.65	79.48	71.62	75.96	75.24	71.36	84.26	79.41	71.40	79.66	68.92
MLS	99.12	3.60	93.33	33.93	79.87	74.86	85.81	56.68	93.82	33.03	96.58	18.97	91.42	36.85
Energy	99.38	2.13	93.83	31.25	78.33	78.86	86.24	56.10	95.32	24.89	97.50	13.26	91.77	34.42
Mahalanobis	99.85	0.53	97.29	12.80	85.08	63.78	91.26	35.45	98.44	8.10	98.67	6.67	95.10	21.22
Residual	99.36	2.70	85.09	63.99	63.92	86.08	86.92	56.50	95.55	23.38	95.84	23.68	88.68	42.72
Vim	99.48	1.86	94.02	30.06	78.59	78.29	86.75	53.95	95.67	22.96	97.70	12.17	92.03	33.21
NECO	99.43	2.16	93.71	31.78	80.42	73.09	87.26	50.52	95.19	24.22	97.42	14.01	92.24	32.63
KL-matching	94.50	23.48	86.54	55.21	82.74	62.81	79.16	66.66	74.56	80.30	83.53	60.59	83.51	58.18
X-Maha (ours)	99.99	0.04	97.77	10.81	83.67	66.99	96.31	16.67	99.97	0.01	99.95	0.14	96.28	15.78
					VIT_	SMALL_	РАТСН1	6_224						
MSP	96.39	16.72	92.72	37.39	87.58	49.60	82.39	57.10	80.54	68.09	87.52	49.64	87.85	46.42
MLS	99.69	1.44	95.97	21.84	91.96	41.67	92.62	29.45	97.66	14.61	98.77	6.74	96.11	19.29
Energy	99.80	1.13	95.29	27.28	91.55	45.20	93.37	25.75	98.58	8.86	99.28	3.78	96.31	18.67
Mahalanobis	99.91	0.53	99.43	2.35	93.02	35.98	97.15	12.93	99.59	2.35	99.65	1.67	98.12	9.30
Residual	99.93	0.25	96.22	24.49	83.28	64.13	95.96	21.20	99.26	3.78	99.37	2.78	95.67	19.44
Vim	99.84	0.96	95.74	25.12	91.69	44.68	93.78	24.60	98.77	7.65	99.38	3.29	96.53	17.72
NECO	99.77	1.13	96.30	20.92	91.64	41.49	92.86	27.03	97.67	14.01	98.92	5.90	96.19	18.41
KL-matching	98.12	7.73	95.63	20.27	90.16	37.62	85.25	46.40	83.94	56.00	90.77	36.06	90.65	34.01
X-Maha (ours)	100.0	0.00	99.68	1.05	92.24	39.11	99.48	2.44	100.0	0.00	100.0	0.00	98.57	7.10

Table 13: OOD detection performance on ImageNet-LT (ID) on smaller transformers.

Method	Text	ure	Plac	ces	SU	IN	iNatu	ralist	Image	Net-O	Aver	age
Method	AUROC	FPR95	AUROC	FPR95	AUROC	FPR95	AUROC	FPR95	AUROC	FPR95	AUROC	FPR95
				VIT	_TINY_I	РАТСН16	_224					
MSP	78.01	73.35	75.50	78.45	75.30	79.07	87.21	54.52	67.95	87.70	76.80	74.62
MLS	84.44	65.73	78.50	75.84	79.44	75.44	91.83	46.49	76.83	84.55	82.21	69.61
Energy	85.85	60.04	78.76	74.90	80.02	74.11	92.72	42.10	78.73	81.55	83.22	66.54
Mahalanobis	89.61	41.86	79.27	67.26	82.44	63.88	97.62	11.83	80.09	77.30	85.81	52.43
Residual	84.86	56.21	68.21	86.03	69.96	84.55	88.63	49.79	73.94	77.95	77.12	70.91
Vim	86.49	57.06	78.97	74.35	80.27	73.02	93.25	38.66	79.22	80.85	83.64	64.79
NECO	86.84	56.44	79.03	73.47	80.61	72.26	94.78	30.01	79.54	79.75	84.16	52.39
KL-matching	81.97	67.22	77.80	74.27	78.06	73.72	91.59	41.18	72.78	84.35	80.44	68.15
X-Maha (ours)	92.21	29.84	78.40	68.87	81.25	66.86	97.72	11.30	82.43	69.90	86.40	49.35
				VIT_	SMALL_	РАТСН1	6_224					
MSP	82.60	60.11	81.41	66.59	81.97	63.84	94.31	25.69	77.74	73.60	83.61	57.97
MLS	87.94	50.51	84.97	60.73	86.46	56.44	96.63	17.04	84.64	65.40	88.13	50.02
Energy	88.96	46.03	85.45	58.10	87.20	53.27	97.09	14.06	85.91	60.85	88.92	46.46
Mahalanobis	91.13	36.06	86.30	54.87	89.54	46.81	99.03	4.49	87.74	55.45	90.75	<u>39.54</u>
Residual	88.66	45.11	79.43	70.30	84.29	60.89	96.18	20.30	82.07	65.85	86.12	52.49
Vim	89.38	44.08	85.72	56.97	87.57	52.06	97.39	12.38	86.29	59.25	89.27	44.95
NECO	89.72	43.40	85.86	56.63	88.18	51.50	98.07	9.36	87.00	58.40	89.77	43.86
KL-matching	86.01	50.67	83.63	60.68	84.80	56.71	96.68	14.62	81.90	65.35	86.60	49.61
X-Maha (ours)	93.35	25.94	86.18	55.21	89.52	46.74	99.13	3.99	89.13	50.20	91.46	36.42

A.7 Ablation studies on OpenOOD v1.5 benchmark

We conducted our experiment again using the Openood v1.5 [59] benchmark and chose Imagenet-1K-LT as the ID dataset, as shown in Table 17. From our experience, this approach is comparable to using ImageNet-1k while being more time-efficient. Our results surpassed those of all other methods by a significant margin on average, highlighting the success of our X-Maha strategy.

A.8 Experiments on OpenOOD v1.5 benchmark

Table 18 presents a comprehensive evaluation of the EVA model's out-of-distribution detection performance using the ImageNet-LT dataset under the OpenOOD v1.5 evaluation framework.

A.9 Ablation studies on varying parameter-efficient fine-tuning methods.

X-Maha is a general framework in which many lightweight fine-tuning methods can be integrated. In addition to Adaptformer [4] which is used in our experiments by default, we test X-Maha with another 5 parameter-efficient fine-tuning (PEFT) methods as well as full fine-tuning. Specifically, we combine X-Maha with *Bias-tuning* [58], *VPT-shallow* [21], *VPT-deep* [21], *LoRA* [18], and *Adapter*

Table 14: OOD detection performance on ImageNet-LT (ID) and five OOD datasets using the zero-shot models without fine-tuning.

Method	Text	ure	Plac	ces	SU	N	iNatu	ralist	Imagel	Net-O	Aver	age
Method	AUROC	FPR95	AUROC	FPR95	AUROC	FPR95	AUROC	FPR95	AUROC	FPR95	AUROC	FPR95
			IMA	GENET-	21K PRE	-TRAINI	ED VIT-S	MALL				
MSP	82.24	58.21	77.75	75.34	78.32	74.35	92.41	37.39	74.87	75.70	81.12	64.20
MLS	91.03	38.14	82.05	66.33	85.45	60.21	96.08	24.66	85.79	66.60	88.08	51.19
Energy	91.76	33.60	82.07	64.62	85.92	56.38	96.00	25.85	86.59	63.60	88.47	48.81
Mahalanobis	92.94	26.74	80.88	68.96	85.09	60.41	98.59	6.10	88.12	53.75	89.12	43.19
Residual	89.39	43.03	61.84	89.78	69.77	84.65	92.23	39.67	80.85	67.70	78.82	64.97
Vim	92.03	32.50	81.99	64.63	85.96	56.15	96.28	23.85	86.91	62.05	88.63	47.84
NECO	92.33	31.10	78.84	69.23	83.22	62.75	97.91	9.57	87.92	56.55	88.05	45.84
KL-matching	85.44	49.66	79.42	72.35	80.89	69.74	94.90	29.76	78.69	67.90	83.87	57.88
X-Maha (ours)	96.57	12.43	78.75	72.76	83.04	63.38	98.28	7.48	90.59	42.60	89.45	39.73
			IMA	AGENET	-21K PRI	E-TRAIN	ED VIT-	TINY				
MSP	76.40	73.71	70.13	86.79	68.43	88.56	82.49	70.08	64.86	87.55	72.46	81.34
MLS	87.68	51.84	73.55	81.88	76.13	82.79	90.23	57.60	77.84	83.25	81.09	71.47
Energy	88.63	46.47	73.36	81.29	76.59	81.44	90.41	56.67	78.99	81.80	81.59	69.53
Mahalanobis	91.78	30.85	73.34	79.18	77.17	76.42	94.89	28.37	80.38	75.75	83.51	58.11
Residual	88.96	43.39	53.28	95.00	56.74	94.70	74.95	79.52	74.57	78.40	69.70	78.20
Vim	89.06	44.47	73.18	81.50	76.48	81.48	90.55	56.22	79.33	81.10	81.72	68.95
NECO	90.04	41.58	72.85	81.42	76.17	81.01	94.23	36.09	80.81	77.30	82.82	63.48
KL-matching	80.83	65.53	71.26	86.35	70.28	88.57	86.62	65.47	69.79	83.85	75.75	77.95
X-Maha (ours)	95.47	17.93	71.78	79.73	74.44	78.06	96.08	20.33	85.39	57.30	84.63	50.67

Table 15: Time consumption (in seconds) comparison between Mahalanobis and X-Maha.

Dataset	Pre-process	ID test set	Texture	Places	SUN	iNaturalist	ImageNet-O	Total
Mahalanobis	685	238	36	61	56	59	14	1149
X-Maha	748	291	38	62	60	61	15	1275

Table 16: Fair comparison with MCM on CIFAR-100, CIFAR-100-LT, and ImageNet-LT ID datasets.

Method	Text	ure	SVI	ΗN	CIF	AR10	Tiny Ima	ageNet	LSU	JN	Place	s365	Aver	age
Method	AUROC	FPR95	AUROC	FPR95	AUROC	FPR95	AUROC	FPR95	AUROC	FPR95	AUROC	FPR95	AUROC	FPR95
						CIFA	R-100							
MCM-untuned	72.98	92.09	90.75	63.39	75.53	88.66	65.54	93.36	50.79	99.11	60.97	97.79	69.43	89.06
MCM-tuned	75.33	91.38	91.55	60.96	75.60	91.03	64.07	95.40	55.14	98.93	63.71	97.67	70.90	89.23
X-Maha (ours)	99.90	0.02	97.41	16.80	85.35	59.44	94.85	27.10	99.89	0.10	99.91	0.03	96.22	17.25
						CIFAR	-100-LT							
MCM-untuned	72.98	92.09	90.75	63.39	75.53	88.66	65.54	93.36	50.79	99.11	60.97	97.79	69.43	89.06
MCM-tuned	75.33	91.38	91.55	60.96	75.60	91.03	64.07	95.40	55.14	98.93	63.71	97.67	70.90	89.23
X-Maha (ours)	99.94	0.00	98.13	8.99	88.74	52.46	97.31	13.23	99.93	0.05	99.95	0.04	97.33	12.46
Method	-	Texture		Place	es	SU	JN	iNa	aturalist	Ir	nageNet	-O	Avera	ige
Methou	AUR	OC FP	R95 AU	ROC 1	FPR95	AUROC	FPR95	AURO	OC FPR	95 AU	ROC FI	PR95 A	UROC	FPR95
]	IMAGEN	ET-1K-l	LT						
MCM-untun	ed 86.1	11 57	7.77 89	9.77	44.69	92.57	37.59	94.6	1 30.9	1 79	0.51 7:	5.70	88.51	49.33
MCM-tuned	85.6	64 60	.11 89	9.82	44.32	92.92	36.25	94.2	6 32.0	1 79	.26 70	6.10	88.38	49.76
X-Maha (our	rs) 89. 9	94 46	.79 9	0.47	42.51	92.71	37.95	94.7	9 27.5	57 82	.94 69	9.10	90.17	44.78

[16]. We report the empirical results for CIFAR-100 in Table 19, CIFAR-100-LT in Table 20, and ImageNet-LT in Table 21. From the results, we observe that X-Maha consistently improves the baselines by a large margin, showing its robustness to the PEFT methods.

Limitations and Broader Impacts

Limitations Despite X-Maha's superior performance compared to the existing methods, it exhibits certain limitations, and there are several unexplored research avenues. For example, the current algorithm only provides a simple approach to calculate Transformer feature mixing weights, which might not be optimal. In addition, our method assumes consistent feature dimensions across all layers, which limits the applicability for more neural network architectures.

Table 17: OOD detection performance on ImageNet-LT (ID) on OpenOOD v1.5.

Method	NIN	CO	Openin	age-O	SSB-	-Hard	iImage	Net-C	Imagel	Net-ES	iImage	Net-R	Imagel	Net-V2	Aver	age
Method	AUROC	FPR95	AUROC	FPR95	AUROC	FPR95	AUROC	FPR95	AUROC	FPR95	AUROC	FPR95	AUROC	FPR95	AUROC	FPR95
						IMAGEN	ЕТ-21К	PRE-TR	AINED V	ΙT						
MSP	87.81	50.02	93.72	27.51	76.72	68.43	67.91	78.58	69.35	69.26	79.73	59.15	57.57	89.92	76.12	63.27
MLS	91.59	42.80	96.28	18.65	81.25	63.86	70.54	76.77	72.11	66.79	83.65	53.22	57.86	90.09	79.04	58.88
Energy	92.12	39.62	96.80	16.02	81.87	61.53	70.80	76.02	72.44	66.06	84.25	50.52	57.79	90.19	79.44	57.14
Mahalanobis	94.00	32.51	97.58	12.61	85.01	52.17	73.93	72.64	73.04	67.08	85.32	48.95	58.02	90.81	80.99	53.83
Residual	83.87	62.45	92.41	33.88	84.87	56.19	74.96	78.03	65.25	82.87	75.05	76.46	53.03	94.38	75.63	69.18
Vim	92.29	38.65	96.94	15.32	82.36	60.40	71.19	75.39	72.47	65.98	84.37	50.20	57.79	90.15	79.63	56.58
NECO	91.97	38.09	96.90	15.19	84.81	54.96	70.55	75.48	72.01	67.61	82.43	53.86	56.86	90.44	79.36	56.52
KL-matching	90.53	41.63	95.95	18.15	79.52	63.02	70.03	75.91	71.54	66.35	82.56	52.60	58.33	89.85	78.35	58.22
X-Maha (ours)	94.98	26.74	98.21	9.72	86.34	49.46	83.96	53.57	76.78	63.45	88.49	42.85	58.36	91.36	83.88	48.16
							CLIP-	VIT-B/1	6							
MSP	80.11	68.94	88.22	46.72	68.06	83.66	73.44	70.44	70.31	68.46	77.27	64.00	57.12	90.78	73.50	70.43
MLS	84.17	67.11	92.93	35.17	71.99	82.44	77.66	67.65	75.66	64.21	84.61	55.96	58.24	90.38	77.89	66.13
Energy	84.15	67.78	93.73	30.59	72.25	82.43	78.02	67.13	76.51	62.51	85.87	52.26	58.22	90.28	78.39	64.71
Mahalanobis	75.13	83.28	86.95	63.82	66.11	89.49	82.68	62.64	84.27	52.46	90.02	47.33	58.18	90.31	77.62	69.90
Residual	61.56	91.54	70.43	81.35	61.00	92.63	82.86	68.28	86.30	54.65	86.28	57.41	56.47	92.06	72.13	76.85
Vim	83.91	68.20	93.57	31.15	72.28	82.57	78.85	65.06	77.52	60.34	86.73	49.79	58.35	89.88	78.74	63.86
NECO	880.96	71.90	92.48	37.13	69.22	85.10	77.84	68.17	78.69	61.76	86.00	54.92	58.18	89.83	77.63	66.97
KL-matching	83.21	66.88	92.13	34.08	70.63	81.75	76.09	67.07	72.92	64.25	81.70	55.46	57.83	90.51	76.36	65.71
X-Maha (ours)	8.30	74.67	92.90	36.93	71.64	81.79	85.49	50.94	87.84	43.49	88.76	50.31	58.22	89.50	80.45	61.09

Table 18: OOD detection performance on ImageNet-LT (ID) on OpenOOD v1.5 on EVA.

Method	NIN AUROC		Openin AUROC		SSB-I AUROC		iImage AUROC		ImageN AUROC		iImage AUROC		ImageN AUROC		Aver AUROC	
						EVA02	2-SMAL	L-PAT	CH14-33	6						
MSP	85.42	58.74	93.96	28.32	67.21	81.62	71.52	70.71	71.12	65.98	82.42	50.02	56.44	90.10	75.44	63.64
MLS	85.22	59.42	93.98	28.32	66.81	81.78	70.94	71.24	72.48	65.16	82.91	49.36	56.44	90.19	75.54	63.64
Energy	60.93	89.79	70.32	86.76	51.36	95.11	50.30	95.21	70.05	74.32	71.41	79.83	51.72	93.81	60.87	87.83
Mahalanobis	88.50	52.47	95.35	24.99	73.67	73.68	74.99	66.73	74.17	64.15	86.59	47.58	57.97	90.15	78.75	59.97
Residual	46.13	99.22	61.80	96.84	48.91	95.38	59.63	92.57	57.34	91.72	64.01	89.43	48.01	96.41	55.12	94.51
Vim	46.94	99.00	63.01	96.48	49.00	95.31	59.52	92.49	58.76	91.23	65.12	88.46	48.13	96.33	54.52	94.87
NECO	79.29	63.75	93.32	28.33	61.44	83.42	68.80	72.11	70.25	66.85	81.47	49.12	54.27	91.34	72.69	64.99
KNN	85.02	68.02	93.33	39.61	68.99	86.43	74.23	68.85	75.50	63.43	86.55	45.53	57.85	90.52	77.35	66.06
NNguide	84.97	68.02	93.33	39.47	68.90	86.47	74.11	68.92	75.67	63.36	86.58	45.44	57.83	90.52	77.34	66.03
RelativeMaha	89.44	50.54	95.04	25.24	74.26	73.55	73.82	68.31	73.32	64.74	85.49	48.87	58.37	89.66	78.53	60.13
KL-matching	12.43	99.97	7.23	99.99	27.79	98.64	27.30	99.01	26.64	98.68	13.68	99.77	42.69	96.04	22.54	98.87
X-Maha	88.71	51.72	95.50	24.17	74.39	72.80	76.70	65.17	74.30	64.14	87.15	46.55	58.12	90.09	79.27	59.23

Broader Impacts This study falls within the domain of out-of-distribution (OOD) detection, a machine learning paradigm that aims to achieve superior classification performance in known classes while identifying OOD samples. Consequently, as this technique gains efficacy and wider adoption, the necessity for extensive data annotation may get diminished, potentially contributing to a rise in unemployment among data annotation professionals.

Table 19: OOD detection performance in terms of AUROC (\uparrow) and FPR95 (\downarrow) for different PEFT methods, and full fine-tuning on CIFAR-100 dataset.

25.42.1	Text	ture	SV	HN	CIFA	R10	Tiny Im	ageNet	LS	JN	Pla	ces	Aver	age
Method							AUROC							
Bias-tuning														
+ MSP	97.46	12.77	94.72	27.13	94.19	29,44	88.42	44.58	86.25	64.76	91.93	41.80	92.16	36.75
+ MLS	99.71	1.24	96.60	13.31	96.96	14.23	94.69	22.00	98.07	10.86	98.73	6.84	97.46	11.41
+ Energy	99.82	0.87	96.62	12.60	97.07	13.58	95.10	20.07	98.72	6.86	99.11	4.74	97.74	9.79
+ Mahalanobis	99.93	0.34	98.80	5.32	96.18	20.60	97.31	10.71	99.58	1.32	99.45	2.68	98.54	6.83
+ Residual	99.98	0.04	97.20	16.92	90.96	49.13	98.46	6.69	99.90	0.14	99.81	0.59	97.72	12.25
+ Vim	99.85	0.74	96.84	11.84	97.09	13.58	95.48	18.94	98.96	5.21	99.24	3.90	97.91	9.04
+ NECO	99.77	1.21	97.03	12.42	96.95	15.77	94.97	20.55	98.34	10.19	98.84	6.58	97.65	11.12
+ X-Maha (ours)	100.0	0.00	99.44	2.29	95.32	25.35	99.68	1.52	99.99	0.01	99.99	0.02	99.07	4.87
VPT-shallow														
+ MSP	95.84	18.09	93.78	34.50	92.09	37.35	85.90	49.15	79.15	78.05	87.17	54.51	88.99	45.27
+ MLS	98.77	5.28	96.55	18.36	94.42	25.10	86.29	47.31	88.68	59.55	92.94	35.22	92.24	31.81
+ Energy	99.04	4.57	96.58	15.87	94.42	24.75	85.83	51.00	89.64	55.53	93.47	32.64	93.16	30.73
+ Mahalanobis	99.97	0.18	92.41	44.63	93.84	32.15	98.04	9.23	99.86	0.18	99.77	0.88	<u>97.31</u>	14.54
+ Residual	99.98	0.05	80.46	67.16	86.92	55.54	99.02	5.17	99.95	0.10	99.89	0.37	94.37	21.40
+ Vim	99.29	3.62	96.71	15.16	94.57	24.64	87.34	45.83	91.64	46.32	94.70	26.97	94.04	27.09
+ NECO	99.30	3.56	95.99	25.70	95.02	24.55	90.59	34.88	94.24	34.05	96.17	20.60	95.22	23.89
+ X-Maha (ours)	100.0	0.00	94.28	36.41	92.37	38.48	99.78	1.15	99.99	0.01	99.98	0.06	97.73	12.68
VPT-deep														
+ MSP	97.43	13.49	91.72	44.53	94.33	30.07	86.93	48.16	84.23	69.02	91.10	47.98	90.79	42.21
+ MLS	99.69	12.49	96.55	15.98	91.21	30.65	95.81	25.68	97.51	13.26	97.51	13.26	96.34	16.59
+ Energy	99.79	1.12	97.59	10.49	96.53	15.82	91.43	29.60	96.53	21.24	97.95	11.21	96.64	14.91
+ Mahalanobis	99.94	0.30	94.27	39.67	96.08	22.59	97.10	162.99	99.08	4.88	99.16	4.47	<u>97.60</u>	14.15
+ Residual	99.97	0.04	91.25	53.35	89.88	50.67	98.07	10.16	99.69	0.74	99.58	1.64	96.41	19.43
+ Vim	99.83	0.83	97.68	10.13	96.57	15.91	92.09	27.75	97.05	18.26	98.22	9.96	96.91	<u>13.81</u>
+ NECO	99.72	1.44	96.53	17.02	96.71	17.06	92.73	26.10	96.80	20.68	98.03	11.12	96.75	15.57
+ X-Maha (ours)	99.99	0.02	96.36	25.31	95.33	26.39	99.59	2.03	99.95	0.00	99.93	0.18	98.52	8.99
LoRA	0.77.0.6		0405		0.4.0.6	20.40	0.00	46.00	0.4.77.6		00.05		04.50	20.75
+ MSP	97.36	12.77	94.85	29.23	94.36	29.49	87.26	46.89	84.76	68.83	90.95	45.35	91.59	38.76
+ MLS	99.57	1.91	97.88	8.89	96.98	14.76	89.51	34.34	95.70	27.11	97.68	12.53	96.22	16.59
+ Energy	99.68	1.38	98.09	7.79	97.09	14.28	89.57	34.75	96.37	23.26	98.09	10.67	96.48	15.36
+ Mahalanobis	99.96	0.11	99.33	2.69	96.65	17.98	97.72	9.47	99.39	2.07	99.47	2.35	98.76	5.78
+ Residual	99.99	0.02	98.15	9.65	91.25	44.12	98.85	4.83	99.84	0.14	99.80	0.45	97.98	9.87
+ Vim	99.75	1.13	98.29	6.91	97.121	14.25	90.50	32.38	96.96	20.00	98.38	9.27	96.83	13.99
+ NECO	99.69 100.0	1.67 0.00	98.43 99.78	6.15 0.88	96.98 95.99	15.96 21.52	91.95 99.82	27.74 0.96	96.66 99.99	21.84 0.00	98.17 99.99	9.97 0.01	96.98 99.26	13.89 3.89
+ X-Maha (ours)	100.0	0.00	99.78	0.88	93.99	21.32	99.82	0.96	99.99	0.00	99.99	0.01	99.20	3.69
Adapter + MSP	97.34	12.54	95.56	23.93	91.73	38.80	85.30	48.04	84.70	62.47	90.66	42.81	90.88	38.10
+ MLS	99.90	0.32	98.31	8.01	94.26	29.06	92.18	29.58	99.10	3.69	99.50	1.51	97.21	12.03
+ MLS + Energy	99.90	0.32	98.28	7.56	94.20	34.00	92.18	28.42	99.10	1.43	99.30	0.61	97.21	12.03
	99.93	0.18	99.44	1.82	95.04	26.43	92.43	9.60	99.46	1.43	99.71	1.36	98.53	6.85
+ Mahalanobis + Residual	99.97	0.12	97.78	14.80	86.21	64.68	98.51	6.91	99.33	0.47	99.03	0.36	97.03	14.54
+ Vim	99.95	0.02	98.48	6.36	93.77	33.18	93.09	26.10	99.57	0.47	99.75	0.36	97.03	11.20
+ VIIII + NECO	99.93	0.10	98.60	6.92	94.41	27.76	92.31	26.44	98.91	6.70	99.73	2.68	97.44	11.82
+ X-Maha (ours)	100.0	0.00	99.50	2.54	96.79	18.07	99.72	1.50	100.0	0.00	100.0	0.00	99.33	3.68
	100.0	0.00	77.50	2.5	70.77	10.07	77.12	1.50	100.0	0.00	100.0	0.00	,,,,,,	
Full fine-tuning + MSP	97.24	15.39	91.45	46.78	93.64	33.62	87.79	48.74	85.44	72.87	91.58	48.41	91.19	44.30
+ MLS	97.24	1.12	90.65	36.84	95.64	16.03	90.43	30.61	97.84	11.13	98.97	3.63	91.19	15.56
+ IVILS + Energy	99.72	0.89	90.63	38.61	96.53	15.89	90.43	30.36	98.11	9.60	98.97	3.08	95.75	16.40
+ Mahalanobis	99.76	0.89	96.80	16.06	96.37	15.38	90.47	13.26	98.11	16.25	98.96	6.61	93.73 97.94	11.35
+ Residual	99.87	0.33	98.13	9.62	95.11	26.57	99.13	4.86	97.69	1.04	98.96	0.54	97.94 98.65	7.13
+ Vim	99.98	0.12	91.57	34.06	95.11	15.50	91.95	25.90	98.39	7.19	99.80	2.27	96.27	14.25
+ VIIII + NECO	99.82	1.33	93.01	31.88	96.96	15.53	92.41	26.21	98.39	17.86	98.78	6.72	96.27	16.59
+ X-Maha (ours)	99.71	0.32	97.12	14.56	96.90	15.18	97.92	11.72	98.64	8.87	99.40	3.41	98.32	9.01
T A-Ivialia (Ouls)	22.23	0.52	71.12	14.50	70.71	15.10	71.7∠	11.72	70.U 1	0.07	22. 4 0	3.41	<u> 70.32</u>	2.01

Table 20: OOD detection performance in terms of AUROC (\uparrow) and FPR95 (\downarrow) for different PEFT methods, and full fine-tuning on CIFAR-100-LT dataset.

Bias-tuning	97.23 99.89 99.93 99.96 99.97 99.95 99.89 100.0 99.43 99.61 99.92 99.72 199.70 100.0 96.78 99.88 99.98 99.98 99.98 99.98 99.98 99.98 99.99 99.89 99.89 99.89 99.89 99.89 99.89 99.89 99.89 99.89 99.89 99.89 99.89 99.89 99.89 99.89 99.88 99.88 99.88 99.88 99.88 99.88 99.88 99.88 99.88 99.88 99.88 99.88 99.88 99.88 99.88 99.88 99.99 99.88 99.99 99.88 99.99 99.88 99.99 99.88 99.99 99.88 99.99 99.88 99.88 99.88 99.88 99.88 99.88 99.88 99.88 99.88 99.88 99.88 99.88 99.88 99.88 99.88 99.88 99.88 99.99 99.88 99.88 99.88 99.99 99.88 9	12.91 0.37 0.25 0.20 0.05 0.16 0.51 0.00 22.66 2.85 1.72 0.37 0.28 1.40 1.37 0.02 14.73 0.87 0.55 0.39 0.30 0.50 0.78	95.68 97.73 97.42 99.58 97.74 98.15 99.91 94.31 96.76 96.05 93.09 84.78 96.26 96.04 95.65 92.13 97.75 98.22 95.61 98.00 97.78 99.32	23.01 10.36 13.18 1.27 11.87 10.84 8.82 0.08 32.06 18.52 24.39 38.88 53.96 22.38 24.00 25.96 38.71 11.72 10.55 10.49 23.77 9.27 11.74 2.97	91.66 94.29 93.78 94.59 85.50 93.87 94.32 93.33 88.65 87.77 86.05 91.12 80.83 86.39 89.82 88.82 90.87 90.42 88.92 92.63 82.05 89.13 91.39	38.32 28.15 33.19 28.56 67.10 32.51 27.12 35.86 52.40 54.41 62.46 42.84 40.84 60.61 43.79 50.14 42.17 44.26 54.12 40.93 73.28 53.34 39.08	85.10 93.67 94.14 97.26 98.00 94.67 93.33 99.76 82.64 81.14 79.32 96.48 97.42 81.39 86.69 99.72 83.57 87.38 87.04 95.85 96.25 88.05	49.19 24.36 22.64 10.39 9.44 20.93 22.52 1.18 58.58 64.50 73.40 14.27 13.56 67.38 43.97 1.36 53.66 45.51 49.12 16.72 18.13	83.91 98.87 99.38 99.54 99.77 99.50 98.59 100.0 78.45 93.33 94.82 99.64 99.75 95.97 95.27 99.98 81.08 96.43 97.25 98.81	65.44 5.06 2.08 2.14 0.53 1.49 9.34 0.00 82.38 40.85 31.44 1.34 0.76 24.05 24.19 0.00	89.82 99.29 99.59 99.55 99.74 99.66 99.23 100.0 85.96 95.01 95.72 99.57 99.67 96.55 97.75 99.97	45.37 2.91 1.38 1.84 0.71 0.99 4.02 0.00 59.76 27.59 23.16 1.82 1.35 18.72 16.80 0.04 52.15 12.18 9.25 5.10 3.77 7.80	90.56 97.29 97.37 98.40 96.83 97.57 97.25 98.83 87.50 92.24 91.93 96.64 93.72 92.72 94.05 94.92 94.86 97.39 95.36	39.04 11.87 12.12 7.40 14.95 11.15 12.06 6.19 51.31 34.79 36.09 23.46 32.42 45.60 22.78 22.78 23.37 13.39 20.45
+ MSP 9 + MLS 9 + Energy 9 + Mahalanobis 9 + Residual 9 + Vim 9 + X-Maha (ours) 1 VPT-shallow 9 + MLS 9 + Energy 9 + Mahalanobis 9 + Residual 9 + Vim 9 + NECO 9 + X-Maha (ours) 1 VPT-deep 9 + X-Maha (ours) 1 VPT-deep 9 + MLS 9 + Energy 9 + MAhalanobis 9 + Residual 9 + Vim 9 + NECO 9 + X-Maha (ours) 9 - Residual 9 + Vim 9 + NECO 9 + X-Maha (ours) 9 - Residual 9 + Vim 9 + NECO 9 + X-Maha (ours) 9 - Residual 9 + Vim 9 + NECO 9 + X-Maha (ours) 9 - Residual 9 + Vim 9 + NECO 9 + X-Maha (ours) 9 - Residual 9 + Vim 9 + NECO 9 + Mahalanobis 9 - Residual 9 - Vim 9 - NECO 9 - MAPABA (ours)	99.89 199.96 199.97 199.95 199.97 199.95 199.91 199.91 199.92 199.92 199.72 199.92 199.93 199.86 199.88 199.89 199.86	0.37 0.25 0.20 0.05 0.16 0.51 0.00 22.66 2.85 1.72 0.37 0.28 1.40 1.37 0.02 14.73 0.87 0.55 0.39 0.30 0.50	97.73 97.42 99.58 97.98 97.74 98.15 99.91 94.31 96.76 96.05 93.09 84.78 96.26 96.04 95.65 92.13 97.75 98.22 95.61 98.00 97.78	10.36 13.18 1.27 11.87 10.84 8.82 0.08 32.06 18.52 24.39 38.88 53.96 22.38 24.00 25.96 38.71 11.75 10.49 23.77 9.27	94.29 93.78 94.59 95.50 93.87 94.32 93.33 88.65 87.77 86.05 91.12 80.83 86.39 89.82 90.87 90.42 88.92 92.63 82.05 89.13 91.39	28.15 33.19 28.56 67.10 32.51 27.12 35.86 52.40 54.41 62.46 42.84 70.84 60.61 43.79 50.14 42.17 44.26 54.12 40.93 73.28 53.34	93.67 94.14 97.26 98.00 94.67 93.33 99.76 82.64 81.14 79.32 96.48 97.42 81.39 96.69 99.72 83.57 87.38 87.04 95.85 96.25 88.05	24.36 22.64 10.39 9.44 20.93 22.52 1.18 58.58 64.50 73.40 14.27 13.56 67.38 43.97 1.36 53.66 45.51 49.12 16.72 18.13	98.87 99.38 99.54 99.77 99.50 98.59 100.0 78.45 93.33 94.82 99.64 99.75 95.97 95.27 99.98 81.08 96.43 97.25 98.81	5.06 2.08 2.14 0.53 1.49 9.34 0.00 82.38 40.85 31.44 1.34 0.76 24.05 24.19 0.00 72.16 22.13 16.66 6.74 3.43	99.29 99.59 99.55 99.74 99.66 99.23 100.0 85.96 95.01 95.72 99.57 99.57 99.61 96.55 97.75 99.97	2.91 1.38 1.84 0.71 0.99 4.02 0.00 59.76 27.59 23.16 1.85 18.72 16.80 0.04 52.15 12.18 9.25 5.10 3.77	97.29 97.37 98.40 96.83 97.57 97.25 98.83 87.50 92.24 91.93 96.64 93.72 92.72 94.05 97.36 88.69 94.92 94.92 95.36	11.87 12.12 7.40 14.95 11.15 12.06 6.19 51.31 34.79 36.09 16.59 23.46 32.42 25.69 12.92 45.60 22.78 23.37 13.39 20.45
+ MLS 9 + Energy 9 + Mahalanobis 9 + Residual 9 + Vim 9 + NECO 9 + X-Maha (ours) 1 VPT-shallow 9 + MIS 9 + Energy 9 + Mahalanobis 9 + Residual 9 + Vim 9 + NECO 9 + X-Maha (ours) 1 VPT-deep 9 + MSP 9 + MIS 9 + MIS 9 + Energy 9 + Mahalanobis 9 + Residual 9 + Vim 9 + MECO 9 + MIS 9 + MIS 9 + MIS 9 + MIS 9 + HINECO 9 + WIM 9 + Residual 9 + Vim 9 + Residual 9 + HINECO 9 + X-Maha (ours) 9 LORA 9 + MIS 9 + MIS 9 + MIS 9 + Residual 9 + Vim 9 + NECO 9 + X-Maha (ours) 9 LORA 9 + MIS 9 +	99.89 199.96 199.97 199.95 199.97 199.95 199.91 199.91 199.92 199.92 199.72 199.92 199.93 199.86 199.88 199.89 199.86	0.37 0.25 0.20 0.05 0.16 0.51 0.00 22.66 2.85 1.72 0.37 0.28 1.40 1.37 0.02 14.73 0.87 0.55 0.39 0.30 0.50	97.73 97.42 99.58 97.98 97.74 98.15 99.91 94.31 96.76 96.05 93.09 84.78 96.26 96.04 95.65 92.13 97.75 98.22 95.61 98.00 97.78	10.36 13.18 1.27 11.87 10.84 8.82 0.08 32.06 18.52 24.39 38.88 53.96 22.38 24.00 25.96 38.71 11.75 10.49 23.77 9.27	94.29 93.78 94.59 95.50 93.87 94.32 93.33 88.65 87.77 86.05 91.12 80.83 86.39 89.82 90.87 90.42 88.92 92.63 82.05 89.13 91.39	28.15 33.19 28.56 67.10 32.51 27.12 35.86 52.40 54.41 62.46 42.84 70.84 60.61 43.79 50.14 42.17 44.26 54.12 40.93 73.28 53.34	93.67 94.14 97.26 98.00 94.67 93.33 99.76 82.64 81.14 79.32 96.48 97.42 81.39 96.69 99.72 83.57 87.38 87.04 95.85 96.25 88.05	24.36 22.64 10.39 9.44 20.93 22.52 1.18 58.58 64.50 73.40 14.27 13.56 67.38 43.97 1.36 53.66 45.51 49.12 16.72 18.13	98.87 99.38 99.54 99.77 99.50 98.59 100.0 78.45 93.33 94.82 99.64 99.75 95.97 95.27 99.98 81.08 96.43 97.25 98.81	5.06 2.08 2.14 0.53 1.49 9.34 0.00 82.38 40.85 31.44 1.34 0.76 24.05 24.19 0.00 72.16 22.13 16.66 6.74 3.43	99.29 99.59 99.55 99.74 99.66 99.23 100.0 85.96 95.01 95.72 99.57 99.57 99.61 96.55 97.75 99.97	2.91 1.38 1.84 0.71 0.99 4.02 0.00 59.76 27.59 23.16 1.85 18.72 16.80 0.04 52.15 12.18 9.25 5.10 3.77	97.29 97.37 98.40 96.83 97.57 97.25 98.83 87.50 92.24 91.93 96.64 93.72 92.72 94.05 97.36 88.69 94.92 94.92 95.36	11.87 12.12 7.40 14.95 11.15 12.06 6.19 51.31 34.79 36.09 16.59 23.46 32.42 25.69 12.92 45.60 22.78 23.37 13.39 20.45
+ Energy 9 + Mahalanobis 9 + Residual 9 + NECO 9 + X-Maha (ours) 1 VPT-shallow + MSP 9 + MLS 9 + Mahalanobis 9 + Residual 9 + Vim 9 + NECO 9 + X-Maha (ours) 1 VPT-deep + MSP 9 + MLS 9 + Energy 9 + Mahalanobis 9 + Residual 9 + Vim 9 + NECO 9 + X-Maha (ours) 1 VPT-deep + MSP 9 + MLS 9 + Energy 9 + Mahalanobis 9 + Residual 9 + Vim 9 + NECO 9 + X-Maha (ours) 9 Lora 4 + MSP 9 + MLS 9 + HSEO 9 + K-Residual 9 + Vim 9 + NECO 9 + X-Maha (ours) 9 - Residual 9 + Vim 9 + NECO 9 + MSP 9 + MABALS 9 + HSEO 9 + MABALS 9 + HSEO 9 + MABALS 9 + MILS 9	99.93 99.96 99.97 99.95 99.89 90.00 94.99 99.43 99.92 99.92 99.72 99.72 99.70 100.00 90.67 80.00 90.88 90.98 9	0.25 0.20 0.05 0.16 0.51 0.00 22.66 2.85 1.72 0.28 1.40 1.37 0.02 14.73 0.87 0.55 0.39 0.30 0.50	97.42 99.58 97.98 97.74 98.15 99.91 94.31 96.76 96.05 93.09 84.78 96.26 96.04 95.65 92.13 97.75 98.22 95.61 98.00 97.78	13.18 1.27 11.87 10.84 8.82 0.08 32.06 18.52 24.39 38.88 53.96 22.38 24.00 25.96 38.71 11.72 10.55 10.49 23.77 9.27	93.78 94.59 85.50 93.87 94.32 93.33 88.65 87.77 86.05 91.12 80.83 86.39 89.82 90.87 90.42 88.82 92.63 82.05 89.13 91.39	33.19 28.56 67.10 32.51 27.12 35.86 52.40 54.41 62.46 42.84 70.84 60.61 43.79 50.14 42.17 44.26 54.12 40.93 73.28 53.34	94.14 97.26 98.00 94.67 93.33 99.76 82.64 81.14 79.32 96.48 97.42 81.39 86.69 99.72 83.57 87.38 87.04 95.85 96.25 88.05	22.64 10.39 9.44 20.93 22.52 1.18 58.58 64.50 73.40 14.27 13.56 67.38 43.97 1.36 53.66 45.51 49.12 16.72 18.13	99.38 99.54 99.77 99.50 98.59 100.0 78.45 93.33 94.82 99.64 99.75 95.27 99.98 81.08 96.43 97.25 98.81	2.08 2.14 0.53 1.49 9.34 0.00 82.38 40.85 31.44 1.34 0.76 24.05 24.19 0.00 72.16 22.13 16.66 6.74 3.43	99.59 99.55 99.74 99.66 99.23 100.0 85.96 95.01 95.72 99.57 99.61 96.55 97.75 99.97	1.38 1.84 0.71 0.99 4.02 0.00 59.76 27.59 23.16 1.82 1.35 18.72 16.80 0.04 52.15 12.18 9.25 5.10 3.77	97.37 98.40 96.83 97.57 97.25 98.83 87.50 92.24 91.93 96.64 93.72 94.05 97.36 88.69 94.92 94.86 97.39 95.36	12.12 7.40 14.95 11.15 12.06 6.19 51.31 34.79 36.09 16.59 23.46 32.42 25.69 12.92 45.60 22.78 23.39 20.45
+ Mahalanobis 9 + Residual 9 + Vim 9 + NECO 9 + X-Maha (ours) 1 VPT-shallow + MSP 9 + MLS 9 + Energy 9 + Mahalanobis 1 + NECO 9 + X-Maha (ours) 1 VPT-deep + MSP 9 + MLS 9 + Energy 9 + Mahalanobis 9 + Residual 9 + Vim 9 + Residual 9 + Vim 9 + Residual 9 + Kandalanobis 9 + Residual 9 + Kandalanobis 9 + Residual 9 + NECO 9 + X-Maha (ours) 9 Lora 1 Lora 2 Lora 3 Lora 3 Lora 4 + MSP 9 + MLS 9 + MESCO 9 + X-Maha (ours) 9 Lora 4 + MSP 9 + MLS 9 + Mahalanobis 9 + Residual 9 + Mahalanobis 9 + Residual 9 + Mahalanobis 9 + Residual 9 + NECO 9	99.96 199.97 190.00 100	0.20 0.05 0.16 0.51 0.00 22.66 2.85 1.72 0.37 0.28 1.40 1.37 0.02 14.73 0.87 0.55 0.39 0.39 0.50 0.78	99.58 97.98 97.74 98.15 99.91 94.31 96.76 96.05 93.09 84.78 96.26 96.04 95.65 92.13 97.63 97.75 98.22 95.61 98.00 97.78	1.27 11.87 10.84 8.82 0.08 32.06 18.52 24.39 38.88 53.96 22.38 24.00 25.96 38.71 11.72 10.55 10.49 23.77 9.27	94.59 85.50 93.87 94.32 93.33 88.65 87.77 86.05 91.12 80.83 86.39 89.82 88.82 90.87 90.42 88.92 92.63 82.05 89.13 91.39	28.56 67.10 32.51 27.12 35.86 52.40 54.41 62.46 42.84 70.84 60.61 43.79 50.14 42.17 44.26 54.12 40.93 73.28 73.28 53.34	97.26 98.00 94.67 93.33 99.76 82.64 81.14 79.32 96.48 97.42 81.39 86.69 99.72 83.57 87.38 87.04 95.85 96.25 88.05	10.39 9.44 20.93 22.52 1.18 58.58 64.50 73.40 14.27 13.56 67.38 43.97 1.36 53.66 45.51 49.12 16.72 18.13	99.54 99.77 99.50 98.59 100.0 78.45 93.33 94.82 99.64 99.75 55.97 95.27 99.98 81.08 96.43 97.25 98.81	2.14 0.53 1.49 9.34 0.00 82.38 40.85 31.44 1.34 0.76 24.05 24.19 0.00 72.16 22.13 16.66 6.74 3.43	99.55 99.74 99.66 99.23 100.0 85.96 95.01 95.72 99.57 99.61 196.55 97.75 99.97	1.84 0.71 0.99 4.02 0.00 59.76 27.59 23.16 1.82 1.35 18.72 16.80 0.04 52.15 12.18 9.25 5.10 3.77	98.40 96.83 97.57 97.25 98.83 87.50 92.24 91.93 96.64 92.72 94.05 97.36 88.69 94.92 94.86 97.39 95.36	7.40 14.95 11.15 12.06 6.19 51.31 34.79 36.09 16.59 23.46 32.42 25.69 12.92 45.60 22.78 23.37 13.39 20.45
+ Residual	99.97 99.97 99.89 100.0 94.99 99.41 99.91 99.92 99.72 99.72 99.72 100.0 96.78 99.78 99.88 99.88 99.88 99.90 99.82 99.99	0.05 0.16 0.51 0.00 22.66 2.85 1.72 0.37 0.28 1.40 0.37 0.02 14.73 0.87 0.55 0.39 0.30 0.50	97.98 97.74 98.15 99.91 94.31 96.76 96.05 93.09 84.78 96.26 96.04 95.65 92.13 97.75 98.22 95.61 98.00 97.78	11.87 10.84 8.82 0.08 32.06 18.52 24.39 38.88 53.96 22.38 24.00 25.96 38.71 11.72 10.55 10.49 23.77 9.27 9.21	85.50 93.87 94.32 93.33 88.65 87.77 86.05 91.12 80.83 86.39 89.82 88.82 90.87 90.42 88.92 92.63 82.05 89.13 91.39	67.10 32.51 27.12 35.86 52.40 54.41 62.46 42.84 60.61 43.79 50.14 42.17 44.26 54.12 40.93 73.28 73.28 53.34	98.00 94.67 93.33 99.76 82.64 81.14 79.32 96.48 97.42 81.39 99.72 83.57 87.38 87.04 95.85 96.25 88.05	9.44 20.93 22.52 1.18 58.58 64.50 73.40 14.27 13.56 67.38 43.97 1.36 53.66 45.51 49.12 16.72 18.13	99.77 99.50 98.59 100.0 78.45 93.33 94.82 99.64 99.75 95.97 99.98 81.08 96.43 97.25 98.81 99.23	0.53 1.49 9.34 0.00 82.38 40.85 31.44 1.34 0.76 24.05 24.19 0.00 72.16 22.13 16.66 6.74 3.43	99.74 99.66 99.23 100.0 85.96 95.01 95.72 99.57 99.61 96.55 97.75 99.97 87.71 97.87 98.35 98.94	0.71 0.99 4.02 0.00 59.76 27.59 23.16 1.82 1.35 18.72 16.80 0.04 52.15 12.18 9.25 5.10 3.77	96.83 97.57 97.55 98.83 87.50 92.24 91.93 96.64 93.72 92.72 94.05 97.36 88.69 94.92 94.86 97.39 95.36	14.95 11.15 12.06 6.19 51.31 34.79 36.09 16.59 23.46 32.42 25.69 12.92 45.60 22.78 23.37 13.39 20.45
+ Vim 9 + NECO 9 + X-Maha (ours) 1 VPT-shallow + MSP 9 + MLS 9 + Energy 9 + Mahalanobis 9 + Residual 9 + Vim 9 + NECO 9 + X-Maha (ours) 1 VPT-deep + MSP 9 + MIS 9 + Energy 9 + Mahalanobis 9 + Residual 9 + Vim 9 + Energy 9 + Mahalanobis 9 + Residual 9 + Uim 9 + Energy 9 + Mahalanobis 9 + Residual 9 + Vim 9 + NECO 9 + X-Maha (ours) 9 Lora 1 Lora 2 Lora 3 Lora 3 Lora 4 HMSP 9 + MILS 9 + HEnergy 9 + Mahalanobis 9 + Residual 9 + Vim 9 + NECO 9 + X-Maha (ours) 9 Lora 4 Lora 4 Lora 5 Lora 6 Lora 7 Lora 7 Lora 7 Lora 7 Lora 7 Lora 8 Lora 9 - Henergy 9 - Hahalanobis 9 - Henergy 9 - Hahalanobis 9 - Residual 9 - Henergy 9 - Hahalanobis 9 - Residual 9 - Henergy 9 - Hahalanobis 9 - Residual 9 - Henergy 9 - Hahalanobis 9 - Residual 9 - Henergy 9 - Hahalanobis 9 - Residual 9 - Henergy 9 - Hahalanobis 9 - Residual 9 - Henergy 9 - Hahalanobis 9 - Residual 9 - Henergy 9 - Hahalanobis 9 -	99.95 99.89 100.0 94.99 99.43 99.61 99.92 99.72 99.70 100.0 96.78 99.88 99.88 99.89 99.89 99.89 99.89	0.16 0.51 0.00 22.66 2.85 1.72 0.37 0.28 1.40 1.37 0.02 14.73 0.87 0.55 0.39 0.30 0.50	97.74 98.15 99.91 94.31 96.76 96.05 93.09 84.78 96.26 96.04 95.65 92.13 97.75 98.22 95.61 98.00 97.78	10.84 8.82 0.08 32.06 18.52 24.39 38.88 53.96 22.38 24.00 25.96 38.71 11.72 10.55 10.49 23.77 9.27 11.74	93.87 94.32 93.33 88.65 87.77 86.05 91.12 80.83 86.39 89.82 90.87 90.42 92.63 82.05 89.13 91.39	32.51 27.12 35.86 52.40 54.41 62.46 42.84 70.84 60.61 43.79 50.14 42.17 44.26 54.12 40.93 73.28 53.34	94.67 93.33 99.76 82.64 81.14 79.32 96.48 97.42 81.39 86.69 99.72 83.57 87.38 87.04 95.85 96.25 88.05	20.93 22.52 1.18 58.58 64.50 73.40 14.27 13.56 67.38 43.97 1.36 53.66 45.51 49.12 16.72 18.13	99.50 98.59 100.0 78.45 93.33 94.82 99.64 99.75 95.27 99.98 81.08 96.43 97.25 98.81 99.23	1.49 9.34 0.00 82.38 40.85 31.44 1.34 0.76 24.05 24.19 0.00 72.16 22.13 16.66 6.74 3.43	99.66 99.23 100.0 85.96 95.01 95.72 99.57 99.61 96.55 97.75 99.97 87.71 97.87 98.35 98.94 99.11	0.99 4.02 0.00 59.76 27.59 23.16 1.82 1.35 18.72 16.80 0.04 52.15 12.18 9.25 5.10 3.77	97.57 97.25 98.83 87.50 92.24 91.93 96.64 93.72 92.72 94.05 97.36 88.69 94.92 94.86 97.39 95.36	11.15 12.06 6.19 51.31 34.79 36.09 16.59 23.46 32.42 25.69 12.92 45.60 22.78 23.37 13.39 20.45
+ NECO 9 + X-Maha (ours) 1: VPT-shallow + MSP 9 + MLS 9 + Mahalanobis 9 + Residual 9 + Vim 9 + X-Maha (ours) 1: VPT-deep + MSP 9 + MILS 9 + Energy 9 + Mahalanobis 9 + Residual 9 + Vim 9 + NECO 9 + X-Maha (ours) 9 Lora 4 + MSP 9 + MLS 9 + NECO 9 + X-Maha (ours) 9 Lora 9 + Mahalanobis 9 + Residual 9 + Vim 9 + NECO 9 + X-Maha (ours) 9 Lora 9 + Mahalanobis 9 + Residual 9 + MILS	99.89 100.0 94.99 99.43 99.61 99.92 99.72 99.70 100.0 96.78 99.86 99.89 99.89 99.89 99.89	0.51 0.00 22.66 2.85 1.72 0.37 0.28 1.40 1.37 0.02 14.73 0.87 0.55 0.39 0.30 0.50 0.78	98.15 99.91 94.31 96.76 96.05 93.09 84.78 96.26 96.04 95.65 92.13 97.63 97.75 98.22 95.61 98.00 97.78	8.82 0.08 32.06 18.52 24.39 38.88 53.96 22.38 24.00 25.96 38.71 11.72 10.55 10.49 23.77 9.27 11.74	94.32 93.33 88.65 87.77 86.05 91.12 80.83 86.39 89.82 88.82 90.87 90.42 88.92 92.63 82.05 89.13 91.39	27.12 35.86 52.40 54.41 62.46 42.84 70.84 60.61 43.79 50.14 42.17 44.26 54.12 40.93 73.28 53.34	93.33 99.76 82.64 81.14 79.32 96.48 97.42 81.39 86.69 99.72 83.57 87.38 87.04 95.85 96.25 88.05	22.52 1.18 58.58 64.50 73.40 14.27 13.56 67.38 43.97 1.36 53.66 45.51 49.12 16.72 18.13	98.59 100.0 78.45 93.33 94.82 99.64 99.75 95.27 99.98 81.08 96.43 97.25 98.81 99.23	9.34 0.00 82.38 40.85 31.44 1.34 0.76 24.05 24.19 0.00 72.16 22.13 16.66 6.74 3.43	99.23 100.0 85.96 95.01 95.72 99.57 99.61 96.55 97.75 99.97 87.71 97.87 98.35 98.94	59.76 27.59 23.16 1.82 1.35 18.72 16.80 0.04 52.15 12.18 9.25 5.10 3.77	97.25 98.83 87.50 92.24 91.93 96.64 93.72 92.72 94.05 97.36 88.69 94.92 94.86 97.39 95.36	12.06 6.19 51.31 34.79 36.09 16.59 23.46 32.42 25.69 12.92 45.60 22.78 23.37 13.39 20.45
+ X-Maha (ours) 1 VPT-shallow + MSP 9 + MLS 9 + Energy 9 + Mahalanobis 9 + Residual 9 + Vim 9 + X-Maha (ours) 1 VPT-deep + MSP 9 + MLS 9 + Energy 9 + Mahalanobis 9 + Residual 9 + NECO 9 + X-Maha (ours) 9 LoRA + MSP 9 + MLS 9 + NECO 9 + X-Maha (ours) 9 LoRA + MSP 9 + MLS 9 + Residual 9 + NECO 9 + X-Maha (ours) 9 LoRA + MSP 9 + Energy 9 + Mahalanobis 9 + Residual 9 + Kesidual 9 + NECO 9 + MLS 9 + Residual 9 + MLS 9 + HILS 9 + Residual 9 + NECO 9 + NECO 9 + NECO 9 + NECO 9	94.99 99.43 99.61 99.92 99.72 99.70 100.0 96.78 99.86 99.89 99.90 99.89	0.00 22.66 2.85 1.72 0.37 0.28 1.40 1.37 0.02 14.73 0.87 0.55 0.39 0.30 0.50 0.78	99.91 94.31 96.76 96.05 93.09 84.78 96.26 96.04 95.65 92.13 97.63 97.75 98.22 95.61 98.00 97.78	32.06 18.52 24.39 38.88 53.96 22.38 24.00 25.96 38.71 11.72 10.55 10.49 23.77 9.27	93.33 88.65 87.77 86.05 91.12 80.83 86.39 89.82 88.82 90.87 90.42 88.92 92.63 82.05 89.13 91.39	52.40 54.41 62.46 42.84 70.84 60.61 43.79 50.14 42.17 44.26 54.12 40.93 73.28 53.34	99.76 82.64 81.14 79.32 96.48 97.42 81.39 86.69 99.72 83.57 87.38 87.04 95.85 96.25 88.05	58.58 64.50 73.40 14.27 13.56 67.38 43.97 1.36 53.66 45.51 49.12 16.72 18.13	78.45 93.33 94.82 99.64 99.75 95.97 95.27 99.98 81.08 96.43 97.25 98.81 99.23	82.38 40.85 31.44 1.34 0.76 24.05 24.19 0.00 72.16 62.13 16.66 6.74 3.43	85.96 95.01 95.72 99.57 99.61 96.55 97.75 99.97 87.71 98.35 98.94 99.11	59.76 27.59 23.16 1.82 1.35 18.72 16.80 0.04 52.15 12.18 9.25 5.10 3.77	98.83 87.50 92.24 91.93 96.64 93.72 94.05 97.36 88.69 94.92 94.86 97.39 95.36	51.31 34.79 36.09 16.59 23.46 32.42 25.69 12.92 45.60 22.78 23.37 13.39 20.45
VPT-shallow + MSP 9 + MLS 9 + Energy 9 + Mahalanobis 9 + Residual 9 + Vim 9 + NECO 9 + X-Maha (ours) 1 VPT-deep + MSP 9 + MLS 9 + Mahalanobis 9 + Residual 9 + Vim 9 + NECO 9 + X-Maha (ours) 9 Lora 4 + MSP 9 + NECO 9 + X-Maha (ours) 9 Lora 9 + Mahalanobis 9 + Residual 9 + Vim 9 + NECO 9 + X-Maha (ours) 9 Lora 9 + MILS 9 + Energy 9 + Mahalanobis 9 + Residual 9 + WIMSP 9 + Kesidual 9 + MILS 9 + Residual 9 + NECO 9 + NECO 9 + NECO 9 + NECO 9	94.99 99.43 99.61 99.92 99.72 99.70 100.0 96.78 99.78 99.86 99.88 99.89 99.89	22.66 2.85 1.72 0.37 0.28 1.40 1.37 0.02 14.73 0.87 0.55 0.39 0.30 0.50 0.78	94.31 96.76 96.05 93.09 84.78 96.26 96.04 95.65 92.13 97.63 97.75 98.22 95.61 98.00 97.78	32.06 18.52 24.39 38.88 53.96 22.38 24.00 25.96 38.71 11.72 10.55 10.49 23.77 9.27 11.74	88.65 87.77 86.05 91.12 80.83 86.39 89.82 88.82 90.87 90.42 88.92 92.63 82.05 89.13 91.39	52.40 54.41 62.46 42.84 70.84 60.61 43.79 50.14 42.17 44.26 54.12 40.93 73.28 53.34	82.64 81.14 79.32 96.48 97.42 81.39 86.69 99.72 83.57 87.38 87.04 95.85 96.25 88.05	58.58 64.50 73.40 14.27 13.56 67.38 43.97 1.36 53.66 45.51 49.12 16.72 18.13	78.45 93.33 94.82 99.64 99.75 95.97 95.27 99.98 81.08 96.43 97.25 98.81 99.23	82.38 40.85 31.44 1.34 0.76 24.05 24.19 0.00 72.16 22.13 16.66 6.74 3.43	85.96 95.01 95.72 99.57 99.61 96.55 97.75 99.97 87.71 97.87 98.35 98.94 99.11	59.76 27.59 23.16 1.82 1.35 18.72 16.80 0.04 52.15 12.18 9.25 5.10 3.77	87.50 92.24 91.93 <u>96.64</u> 93.72 94.05 97.36 88.69 94.92 94.86 <u>97.39</u> 95.36	51.31 34.79 36.09 16.59 23.46 32.42 25.69 12.92 45.60 22.78 23.37 13.39 20.45
+ MSP 9 + MLS 9 + Energy 9 + Residual 9 + Vim 9 + NECO 9 + X-Maha (ours) 1 VPT-deep + MSP 9 + MLS 9 + Mahalanobis 9 + Residual 9 + Vim 9 + MAND 9 + MAND 9 + MAND 9 + Company 9 + Company 9 + NECO 9 + X-Maha (ours) 9 LORA 9 + MILS 9 + Energy 9 + Mahalanobis 9 + Residual 9 + Vim 9 + NECO 9 + X-Maha (ours) 9 LORA 9 + MILS 9 + Energy 9 + Mahalanobis 9 + Residual 9 + NECO 9 + NECO 9 + NECO 9 + NECO 9	99.43 99.61 99.92 99.92 99.72 99.70 100.0 96.78 99.78 99.86 99.88 99.89 99.89 99.89	2.85 1.72 0.37 0.28 1.40 1.37 0.02 14.73 0.87 0.55 0.39 0.30 0.50 0.78	96.76 96.05 93.09 84.78 96.26 96.04 95.65 92.13 97.63 97.75 98.22 95.61 98.00 97.78	18.52 24.39 38.88 53.96 22.38 24.00 25.96 38.71 11.72 10.55 10.49 23.77 9.27 11.74	87.77 86.05 91.12 80.83 86.39 89.82 88.82 90.87 90.42 88.92 92.63 82.05 89.13 91.39	54.41 62.46 42.84 70.84 60.61 43.79 50.14 42.17 44.26 54.12 40.93 73.28 53.34	81.14 79.32 96.48 97.42 81.39 86.69 99.72 83.57 87.38 87.04 95.85 96.25 88.05	64.50 73.40 14.27 13.56 67.38 43.97 1.36 53.66 45.51 49.12 16.72 18.13	93.33 94.82 99.64 99.75 95.97 95.27 99.98 81.08 96.43 97.25 98.81 99.23	40.85 31.44 1.34 0.76 24.05 24.19 0.00 72.16 22.13 16.66 6.74 3.43	95.01 95.72 99.57 99.61 96.55 97.75 99.97 87.71 97.87 98.35 98.94 99.11	27.59 23.16 1.82 1.35 18.72 16.80 0.04 52.15 12.18 9.25 5.10 3.77	92.24 91.93 96.64 93.72 92.72 94.05 97.36 88.69 94.92 94.86 97.39 95.36	34.79 36.09 16.59 23.46 32.42 25.69 12.92 45.60 22.78 23.37 13.39 20.45
+ MLS 9 + Energy 9 + Mahalanobis 9 + Residual 9 + Vim 9 + NECO 9 + X-Maha (ours) 1 VPT-deep + MSP 9 + Mahalanobis 9 + Residual 9 + Vim 9 + NECO 9 + X-Maha (ours) 9 Lora + MSP 9 + MLS 9 + NECO 9 + X-Maha (ours) 9 Lora + HMSP 9 + MLS 9 + Mahalanobis 9 + Residual 9 + Wim 9 + NECO 9 + X-Maha (ours) 9	99.43 99.61 99.92 99.92 99.72 99.70 100.0 96.78 99.78 99.86 99.88 99.89 99.89 99.89	2.85 1.72 0.37 0.28 1.40 1.37 0.02 14.73 0.87 0.55 0.39 0.30 0.50 0.78	96.76 96.05 93.09 84.78 96.26 96.04 95.65 92.13 97.63 97.75 98.22 95.61 98.00 97.78	18.52 24.39 38.88 53.96 22.38 24.00 25.96 38.71 11.72 10.55 10.49 23.77 9.27 11.74	87.77 86.05 91.12 80.83 86.39 89.82 88.82 90.87 90.42 88.92 92.63 82.05 89.13 91.39	54.41 62.46 42.84 70.84 60.61 43.79 50.14 42.17 44.26 54.12 40.93 73.28 53.34	81.14 79.32 96.48 97.42 81.39 86.69 99.72 83.57 87.38 87.04 95.85 96.25 88.05	64.50 73.40 14.27 13.56 67.38 43.97 1.36 53.66 45.51 49.12 16.72 18.13	93.33 94.82 99.64 99.75 95.97 95.27 99.98 81.08 96.43 97.25 98.81 99.23	40.85 31.44 1.34 0.76 24.05 24.19 0.00 72.16 22.13 16.66 6.74 3.43	95.01 95.72 99.57 99.61 96.55 97.75 99.97 87.71 97.87 98.35 98.94 99.11	27.59 23.16 1.82 1.35 18.72 16.80 0.04 52.15 12.18 9.25 5.10 3.77	92.24 91.93 96.64 93.72 92.72 94.05 97.36 88.69 94.92 94.86 97.39 95.36	34.79 36.09 16.59 23.46 32.42 25.69 12.92 45.60 22.78 23.37 13.39 20.45
+ Energy 9 + Mahalanobis 9 + Residual 9 + NECO 9 + X-Maha (ours) 1 VPT-deep + MSP 9 + Malalanobis 9 + Residual 9 + Vim 9 + NECO 9 + X-Maha (ours) 9 Lora 4 - MSP 9 + MLS 9 + MES 9 + Kesidual 9 + Vim 9 + NECO 9 + X-Maha (ours) 9 - Residual 9 + Vim 9 + NECO 9 + X-Maha (ours) 9 - Residual 9 - Wim 9 -	99.61 99.92 99.92 99.72 99.70 100.0 96.78 99.78 99.86 99.88 99.90 99.89 99.89	1.72 0.37 0.28 1.40 1.37 0.02 14.73 0.87 0.55 0.39 0.30 0.50 0.78	96.05 93.09 84.78 96.26 96.04 95.65 92.13 97.65 98.22 95.61 98.00 97.78	24.39 38.88 53.96 22.38 24.00 25.96 38.71 11.72 10.55 10.49 23.77 9.27 11.74	86.05 91.12 80.83 86.39 89.82 88.82 90.87 90.42 88.92 92.63 82.05 89.13 91.39	62.46 42.84 70.84 60.61 43.79 50.14 42.17 44.26 54.12 40.93 73.28 53.34	79.32 96.48 97.42 81.39 86.69 99.72 83.57 87.38 87.04 95.85 96.25 88.05	73.40 14.27 13.56 67.38 43.97 1.36 53.66 45.51 49.12 16.72 18.13	94.82 99.64 99.75 95.97 95.27 99.98 81.08 96.43 97.25 98.81 99.23	31.44 1.34 0.76 24.05 24.19 0.00 72.16 22.13 16.66 6.74 3.43	95.72 99.57 99.61 96.55 97.75 99.97 87.71 97.87 98.35 98.94 99.11	23.16 1.82 1.35 18.72 16.80 0.04 52.15 12.18 9.25 5.10 3.77	91.93 96.64 93.72 92.72 94.05 97.36 88.69 94.92 94.86 <u>97.39</u> 95.36	36.09 16.59 23.46 32.42 25.69 12.92 45.60 22.78 23.37 13.39 20.45
+ Mahalanobis 9 + Residual 9 + Vim 9 + NECO 9 + X-Maha (ours) 1 VPT-deep + MSP 9 + MILS 9 + Energy 9 + Mahalanobis 9 + Residual 9 + NECO 9 + X-Maha (ours) 9 LoRA + MSP 9 + MLS 9 + Energy 9 + Mahalanobis 9 + Residual 9 + Yim 9 + NECO 9 + X-Maha (ours) 9 LoRA 9 + MLS 9 + Energy 9 + Mahalanobis 9 + Residual 9 + Residual 9 + Residual 9 + NECO 9	99.92 99.92 99.72 99.70 100.0 96.78 99.86 99.86 99.88 99.90 99.89	0.37 0.28 1.40 1.37 0.02 14.73 0.87 0.55 0.39 0.30 0.50 0.78	93.09 84.78 96.26 96.04 95.65 92.13 97.63 97.75 98.22 95.61 98.00 97.78	38.88 53.96 22.38 24.00 25.96 38.71 11.72 10.55 10.49 23.77 9.27 11.74	91.12 80.83 86.39 89.82 88.82 90.87 90.42 88.92 92.63 82.05 89.13 91.39	42.84 70.84 60.61 43.79 50.14 42.17 44.26 54.12 40.93 73.28 53.34	96.48 97.42 81.39 86.69 99.72 83.57 87.38 87.04 95.85 96.25 88.05	14.27 13.56 67.38 43.97 1.36 53.66 45.51 49.12 16.72 18.13	99.64 99.75 95.97 95.27 99.98 81.08 96.43 97.25 98.81 99.23	1.34 0.76 24.05 24.19 0.00 72.16 22.13 16.66 6.74 3.43	99.57 99.61 96.55 97.75 99.97 87.71 97.87 98.35 98.94 99.11	1.82 1.35 18.72 16.80 0.04 52.15 12.18 9.25 5.10 3.77	96.64 93.72 92.72 94.05 97.36 88.69 94.92 94.86 <u>97.39</u> 95.36	16.59 23.46 32.42 25.69 12.92 45.60 22.78 23.37 13.39 20.45
+ Residual	99.92 99.72 99.70 100.0 96.78 99.86 99.86 99.89 99.90 99.89	0.28 1.40 1.37 0.02 14.73 0.87 0.55 0.39 0.30 0.50 0.78	84.78 96.26 96.04 95.65 92.13 97.63 97.75 98.22 95.61 98.00 97.78	53.96 22.38 24.00 25.96 38.71 11.72 10.55 10.49 23.77 9.27 11.74	80.83 86.39 89.82 88.82 90.87 90.42 88.92 92.63 82.05 89.13 91.39	70.84 60.61 43.79 50.14 42.17 44.26 54.12 40.93 73.28 53.34	97.42 81.39 86.69 99.72 83.57 87.38 87.04 95.85 96.25 88.05	13.56 67.38 43.97 1.36 53.66 45.51 49.12 16.72 18.13	99.75 95.97 95.27 99.98 81.08 96.43 97.25 98.81 99.23	0.76 24.05 24.19 0.00 72.16 22.13 16.66 6.74 3.43	99.61 96.55 97.75 99.97 87.71 97.87 98.35 98.94 99.11	1.35 18.72 16.80 0.04 52.15 12.18 9.25 5.10 3.77	93.72 92.72 94.05 97.36 88.69 94.92 94.86 <u>97.39</u> 95.36	23.46 32.42 25.69 12.92 45.60 22.78 23.37 <u>13.39</u> 20.45
+ Vim 9 + NECO 9 + X-Maha (ours) 1 VPT-deep + MSP 9 + MLS 9 + Residual 9 + Vim 9 + NECO 9 + X-Maha (ours) 9 LoRA + MSP 9 + MLS 9 + MES 9 + Mahalanobis 9 + Residual 9 + Vim 9 + NECO 9 + X-Maha (ours) 9	99.72 99.70 100.0 96.78 99.78 99.86 99.89 99.89 99.89 99.89	1.40 1.37 0.02 14.73 0.87 0.55 0.39 0.30 0.50 0.78	96.26 96.04 95.65 92.13 97.63 97.75 98.22 95.61 98.00 97.78	22.38 24.00 25.96 38.71 11.72 10.55 10.49 23.77 9.27 11.74	90.87 90.42 88.92 92.63 82.05 89.13 91.39	60.61 43.79 50.14 42.17 44.26 54.12 40.93 73.28 53.34	81.39 86.69 99.72 83.57 87.38 87.04 95.85 96.25 88.05	67.38 43.97 1.36 53.66 45.51 49.12 16.72 18.13	95.97 95.27 99.98 81.08 96.43 97.25 98.81 99.23	24.05 24.19 0.00 72.16 22.13 16.66 6.74 3.43	96.55 97.75 99.97 87.71 97.87 98.35 98.94 99.11	18.72 16.80 0.04 52.15 12.18 9.25 5.10 3.77	92.72 94.05 97.36 88.69 94.92 94.86 <u>97.39</u> 95.36	32.42 25.69 12.92 45.60 22.78 23.37 <u>13.39</u> 20.45
+ NECO 9 + X-Maha (ours) 1: VPT-deep + MSP 9 + MLS 9 + Energy 9 + Mahalanobis 9 + Residual 9 + NECO 9 + X-Maha (ours) 9 LoRA + MSP 9 + MLS 9 + Energy 9 + MAhalanobis 9 + Energy 9 + Mahalanobis 9 + Residual 9 + Residual 9 + Residual 9 + NECO 9 + NECO 9 + NECO 9 + NECO 9	99.70 100.0 96.78 99.78 99.86 99.88 99.90 99.89 99.89	1.37 0.02 14.73 0.87 0.55 0.39 0.30 0.50 0.78	96.04 95.65 92.13 97.63 97.75 98.22 95.61 98.00 97.78	24.00 25.96 38.71 11.72 10.55 10.49 23.77 9.27 11.74	90.87 90.42 88.92 92.63 82.05 89.13 91.39	43.79 50.14 42.17 44.26 54.12 40.93 73.28 53.34	86.69 99.72 83.57 87.38 87.04 95.85 96.25 88.05	43.97 1.36 53.66 45.51 49.12 16.72 18.13	95.27 99.98 81.08 96.43 97.25 98.81 99.23	24.19 0.00 72.16 22.13 16.66 6.74 3.43	97.75 99.97 87.71 97.87 98.35 98.94 99.11	16.80 0.04 52.15 12.18 9.25 5.10 3.77	94.05 97.36 88.69 94.92 94.86 <u>97.39</u> 95.36	25.69 12.92 45.60 22.78 23.37 13.39 20.45
+ X-Maha (ours) 1 VPT-deep + MSP 9 + MLS 9 + Energy 9 + Mahalanobis 9 + Residual 9 + NECO 9 + X-Maha (ours) 9 LoRA + MSP 9 + MLS 9 + Energy 9 + Mahalanobis 9 + Esergy 9 + Kesidual 9 + Residual 9 + NECO 9 + NECO 9 + X-Maha (ours) 1	96.78 99.78 99.86 99.88 99.90 99.89 99.89	0.02 14.73 0.87 0.55 0.39 0.30 0.50 0.78	95.65 92.13 97.63 97.75 98.22 95.61 98.00 97.78	38.71 11.72 10.55 10.49 23.77 9.27 11.74	90.87 90.42 88.92 92.63 82.05 89.13 91.39	50.14 42.17 44.26 54.12 40.93 73.28 53.34	99.72 83.57 87.38 87.04 95.85 96.25 88.05	53.66 45.51 49.12 16.72 18.13	99.98 81.08 96.43 97.25 98.81 99.23	72.16 22.13 16.66 6.74 3.43	99.97 87.71 97.87 98.35 98.94 99.11	52.15 12.18 9.25 5.10 3.77	97.36 88.69 94.92 94.86 97.39 95.36	45.60 22.78 23.37 13.39 20.45
VPT-deep + MSP 9 + MLS 9 + Energy 9 + Mahalanobis 9 + Residual 9 + Vim 9 + NECO 9 + X-Maha (ours) 9 LoRA 9 + MLS 9 + MLS 9 + MLS 9 + MLS 9 + Energy 9 + Mahalanobis 9 + Residual 9 + Residual 9 + NECO 9 + NECO 9 + X-Maha (ours) 1	96.78 99.78 99.86 99.88 99.90 99.89 99.82	14.73 0.87 0.55 0.39 0.30 0.50 0.78	92.13 97.63 97.75 98.22 95.61 98.00 97.78	38.71 11.72 10.55 10.49 23.77 9.27 11.74	90.87 90.42 88.92 92.63 82.05 89.13 91.39	42.17 44.26 54.12 40.93 73.28 53.34	83.57 87.38 87.04 95.85 96.25 88.05	53.66 45.51 49.12 16.72 18.13	81.08 96.43 97.25 98.81 99.23	72.16 22.13 16.66 6.74 3.43	87.71 97.87 98.35 98.94 99.11	52.15 12.18 9.25 5.10 3.77	88.69 94.92 94.86 <u>97.39</u> 95.36	45.60 22.78 23.37 13.39 20.45
+ MSP 9 + MILS 9 + Energy 9 + Mahalanobis 9 + Residual 9 + Vim 9 + NECO 9 + X-Maha (ours) 9 LoRA 9 + MLS 9 + MLS 9 + Energy 9 + Mahalanobis 9 + Residual 9 + Residual 9 + NECO 9 + NECO 9 + X-Maha (ours) 1	99.78 99.86 99.88 99.90 99.89 99.82 99.99	0.87 0.55 0.39 0.30 0.50 0.78	97.63 97.75 98.22 95.61 98.00 97.78	11.72 10.55 10.49 23.77 9.27 11.74	90.42 88.92 92.63 82.05 89.13 91.39	44.26 54.12 40.93 73.28 53.34	87.38 87.04 95.85 96.25 88.05	45.51 49.12 16.72 18.13	96.43 97.25 98.81 99.23	22.13 16.66 6.74 3.43	97.87 98.35 98.94 99.11	12.18 9.25 5.10 3.77	94.92 94.86 <u>97.39</u> 95.36	22.78 23.37 13.39 20.45
+ MLS 9 + Energy 9 + Mahalanobis 9 + Residual 9 + Vim 9 + NECO 9 + X-Maha (ours) 9 LoRA 9 + MLS 9 + Energy 9 + Mahalanobis 9 + Residual 9 + Residual 9 + Vim 9 + NECO 9 + X-Maha (ours) 1	99.78 99.86 99.88 99.90 99.89 99.82 99.99	0.87 0.55 0.39 0.30 0.50 0.78	97.63 97.75 98.22 95.61 98.00 97.78	11.72 10.55 10.49 23.77 9.27 11.74	90.42 88.92 92.63 82.05 89.13 91.39	44.26 54.12 40.93 73.28 53.34	87.38 87.04 95.85 96.25 88.05	45.51 49.12 16.72 18.13	96.43 97.25 98.81 99.23	22.13 16.66 6.74 3.43	97.87 98.35 98.94 99.11	12.18 9.25 5.10 3.77	94.92 94.86 <u>97.39</u> 95.36	22.78 23.37 13.39 20.45
+ Energy 9 + Mahalanobis 9 + Residual 9 + Vim 9 + NECO 9 + X-Maha (ours) 9 LoRA + MSP 9 + MLS 9 + Energy 9 + Mahalanobis 9 + Residual 9 + Vim 9 + NECO 9 + NECO 9 + X-Maha (ours) 1	99.86 99.88 99.90 99.89 99.82 99.99	0.55 0.39 0.30 0.50 0.78	97.75 98.22 95.61 98.00 97.78	10.55 10.49 23.77 9.27 11.74	88.92 92.63 82.05 89.13 91.39	54.12 40.93 73.28 53.34	87.04 95.85 96.25 88.05	49.12 16.72 18.13	97.25 98.81 99.23	16.66 6.74 3.43	98.35 98.94 99.11	9.25 5.10 3.77	94.86 <u>97.39</u> 95.36	23.37 13.39 20.45
+ Mahalanobis 9 + Residual 9 + Vim 9 + NECO 9 + X-Maha (ours) 9 Lora + MSP 9 + MLS 9 + Energy 9 + Mahalanobis 9 + Residual 9 + Residual 9 + NECO 9 + X-Maha (ours) 1	99.88 99.90 99.89 99.82 99.99	0.39 0.30 0.50 0.78	98.22 95.61 98.00 97.78	10.49 23.77 9.27 11.74	92.63 82.05 89.13 91.39	40.93 73.28 53.34	95.85 96.25 88.05	16.72 18.13	98.81 99.23	6.74 3.43	98.94 99.11	5.10 3.77	97.39 95.36	$\frac{13.39}{20.45}$
+ Residual 9 + Vim 9 + NECO 9 + X-Maha (ours) 9 Lora + MSP 9 + MLS 9 + Energy 9 + Mahalanobis 9 + Residual 9 + Vim 9 + NECO 9 + X-Maha (ours) 1	99.90 99.89 99.82 99.99	0.30 0.50 0.78	95.61 98.00 97.78	23.77 9.27 11.74	82.05 89.13 91.39	73.28 53.34	96.25 88.05	18.13	99.23	3.43	99.11	3.77	95.36	20.45
+ Vim 9 + NECO 9 + X-Maha (ours) 9 Lora + MSP 9 + MLS 9 + Energy 9 + Mahalanobis 9 + Residual 9 + Vim 9 + NECO 9 + X-Maha (ours) 1	99.89 99.82 99.99	0.50 0.78	98.00 97.78	9.27 11.74	89.13 91.39	53.34	88.05							
+ NECO 9 + X-Maha (ours) 9 LoRA + MSP 9 + MLS 9 + Energy 9 + Residual 9 + Residual 9 + Vim 9 + NECO 9 + X-Maha (ours) 1	99.82 99.99	0.78	97.78	11.74	91.39			45.00					95.22	21.68
+ X-Maha (ours) 9 LoRA	99.99					39 08			97.68	14.16	98.58			
LoRA + MSP 9 + MLS 9 + Energy 9 + Mahalanobis 9 + Residual 9 + Vim 9 + NECO 9 + X-Maha (ours) 1		0.00	99.32	2.97			89.00	35.93	96.60	18.40	98.14	10.10	95.45	19.34
+ MSP 9 + MLS 9 + Energy 9 + Mahalanobis 9 + Residual 9 + Vim 9 + NECO 9 + X-Maha (ours) 1	06 77				91.05	46.61	99.56	2.10	99.94	0.00	99.92	0.07	98.30	8.62
+ MLS 9 + Energy 9 + Mahalanobis 9 + Residual 9 + Vim 9 + NECO 9 + X-Maha (ours) 1		4505	0.1.10	22.50		44.05	04.06		04.50	=		40.24	00.45	40.50
+ Energy 9 + Mahalanobis 9 + Residual 9 + Vim 9 + NECO 9 + X-Maha (ours) 1	96.77	15.05	94.10	32.79	91.25	41.07	84.06	51.62	81.70	71.24	88.80	49.24	89.45	43.50
+ Mahalanobis 9 + Residual 9 + Vim 9 + NECO 9 + X-Maha (ours) 1	99.78	0.85	96.95	16.78	93.06	32.74	87.54	43.19	97.66	14.45	98.75	6.61	95.62	19.10
+ Residual 9 + Vim 9 + NECO 9 + X-Maha (ours) 1	99.84	0.44	96.51	20.22	92.28	39.13	87.19	47.63	98.31	9.71	99.09	4.23	95.54	20.23
+ Vim 9 + NECO 9 + X-Maha (ours) 1	99.97 99.98	0.09	99.59	1.12	94.16	30.32	97.26	10.76	99.47 99.74	2.15	99.59	1.55	98.34 96.72	7.66 14.79
+ NECO 9 + X-Maha (ours) 1	99.98	0.07	98.04	11.86	84.77 92.41	66.35 38.74	98.08 88.48	8.99 42.91		0.77	99.72 99.25	0.70 3.28	95.95	
+ X-Maha (ours) 1	99.89	0.39 0.69	97.00 97.89	16.42 11.25	93.25	31.42	89.67	33.65	98.63 97.47	7.75 15.13	98.84	6.11	95.95	18.25 16.38
	100.0	0.09	97.89	0.01	93.23	38.01	99.87	0.59	100.0	0.00	100.0	0.00	98.74	6.43
Adapter	100.0	0.00	22.20	0.01	92.02	36.01	22.01	0.59	100.0	0.00	100.0	0.00	70.74	0.43
	17 24	12.54	05.56	22.02	01.72	20 00	95.20	49.04	94 70	62 47	00.66	12 01	00.00	20 10
	97.34 99.90	12.54 0.32	95.56 98.31	23.93 8.01	91.73 94.26	38.80 29.06	85.30 92.18	48.04 29.58	84.70 99.10	62.47 3.69	90.66 99.50	42.81 1.51	90.88 97.21	38.10 12.03
	99.90	0.32	98.31	7.56	94.26	34.00	92.18	28.42	99.10	1.43	99.50 99.71	0.61	97.21	12.03
	99.93	0.18	98.28 99.44	1.82	95.04	26.43	92.43 97.58	9.60	99.48	1.43	99.71	1.36	98.53	6.85
	99.97	0.12	99.44 97.78	1.82	95.04 86.21	64.68	97.58 98.51	6.91	99.33 99.85	0.47	99.63	0.36	98.53 97.03	14.54
	99.96	0.02	98.48	6.36	93.77	33.18	93.09	26.10	99.83	0.47	99.84	0.36	97.03	11.20
	99.90	0.10	98.60	6.92	94.41	27.76	92.31	26.44	98.91	6.70	99.45	2.68	97.26	11.82
	100.0	0.00	99.92	0.92	94.12	30.70	99.80	0.92	100.0	0.00	100.0	0.00	98.97	5.28
` ′	. 00.0	0.00		0.07	,2	50.70	,,,,,,	0.02	100.0	0.00	100.0	0.00	,,,,,	
Full fine-tuning + MSP 9	96.93	14.29	93.98	32.33	90.46	46.33	83.91	53.60	85.16	66.75	90.43	46,44	90.14	43.29
	99.86	0.50	93.98	33.58	93.96	28.83	88.43	37.80	99.16	1.93	99.41	1.80	95.81	17.41
	99.80	0.34	92.59	47.61	93.90	29.66	88.46	37.68	99.10	0.71	99.41	0.97	95.66	19.49
	99.95	0.27	97.08	16.06	95.14	23.82	97.04	13.62	99.18	5.22	99.52	2.62	97.99	10.27
	99.99	0.27	97.71	13.20	90.08	49.81	98.89	5.16	99.86	0.35	99.91	0.26	97.74	11.47
		0.02	93.63	40.38	93.98	29.20	90.18	32.65	99.65	0.33	99.73	0.25	96.18	17.26
	14 44	0.23	94.73	29.96	94.34	25.66	90.18	31.81	98.75	8.39	99.73	3.89	96.17	16.71
+ X-Maha (ours) 9	99.94 99.87			27.70	95.20	23.66	98.50	38.37	99.81	80.77	99.87	0.58	98.54	7.35

Table 21: OOD detection performance in terms of AUROC (\uparrow) and FPR95 (\downarrow) for different PEFT methods, and full fine-tuning on ImageNet-LT dataset.

	Text	ure	Plac	ces	SU	N	iNatu	ralist	Image!	Net-O	Aver	age
Method					AUROC				AUROC	FPR95		
Bias-tuning												
+ MSP	83.92	58.30	80.95	67.86	81.16	66.33	94.31	26.99	75.83	77.60	83.23	59.42
+ MLS	88.71	49.75	84.46	61.47	85.84	58.57	96.93	16.31	82.68	71.40	87.72	51.50
+ Energy	89.93	43.48	85.15	57.30	86.97	52.85	97.84	10.11	84.22	66.95	88.82	46.14
+ Mahalanobis	87.55	59.63	82.72	61.63	86.38	51.55	97.89	10.11	85.03	62.65	87.92	49.27
+ Residual	73.74	81.88	68.43	82.87	75.65	73.07	88.27	48.56	72.40	80.00	75.70	73.28
+ Vim	90.06	42.68	85.22	57.05	87.16	52.08	97.92	9.83	84.39	66.60	88.95	45.65
+ NECO	88.38	50.51	84.00	60.84	86.25	57.23	97.65	12.16	83.85	67.40	88.03	49.63
+ X-Maha (ours)	90.95	41.45	81.67	63.98	85.48	54.88	97.75	11.44	86.58	56.70	88.48	45.69
VPT-shallow												10102
+ MSP	85.58	49.11	85.44	55.99	86.38	52.79	97.53	10.26	83.79	57.95	87.74	45.22
+ MLS	89.30	41.47	88.52	49.37	90.05	45.47	98.64	5.90	88.74	48.50	91.05	38.14
+ Energy	90.00	37.94	89.01	46.13	90.73	41.65	98.95	4.31	89.69	44.20	91.68	34.85
+ Mahalanobis	92.07	29.52	86.20	58.31	88.98	49.94	99.19	3.10	91.51	38.95	91.59	35.96
+ Residual	88.37	49.73	73.68	80.55	79.27	72.40	96.66	16.66	84.03	60.05	84.40	55.88
+ Vim	90.32	36.33	89.04	46.03	90.82	41.24	99.02	4.11	89.93	42.75	91.83	34.09
+ NECO	91.15	33.32	87.20	49.53	89.67	44.33	99.01	3.86	89.98	43.80	91.40	34.97
+ X-Maha (ours)	95.93	14.54	85.98	57.66	89.03	47.59	99.18	3.17	93.34	32.30	92.69	31.05
VPT-deep												
+ MSP	85.28	49.27	84.75	57.12	85.92	53.82	97.13	11.51	83.13	58.20	87.24	45.98
+ MLS	89.57	40.30	88.37	49.82	89.97	45.76	98.42	6.61	88.35	49.70	90.93	38.44
+ Energy	90.32	37.02	88.92	46.67	90.65	42.09	98.72	5.21	89.23	45.60	91.57	35.32
+ Mahalanobis	92.06	29.38	89.41	46.03	91.53	39.21	99.20	3.07	90.76	41.65	92.59	31.87
+ Residual	89.31	43.60	82.48	65.82	86.52	56.29	97.04	14.73	82.29	62.05	87.53	48.50
+ Vim	90.62	35.25	89.11	45.87	90.88	41.07	98.81	4.86	89.42	44.15	91.77	34.24
+ NECO	90.47	35.04	88.46	46.25	90.73	39.93	98.82	4.56	88.81	45.15	91.46	34.19
+ X-Maha (ours)	95.52	16.03	89.27	46.36	91.57	38.40	99.25	3.07	92.55	35.25	93.63	27.82
LoRA												
+ MSP	85.99	47.75	85.29	56.70	86.36	53.65	97.14	11.87	83.59	58.30	87.67	45.65
+ MLS	90.06	39.08	88.56	50.13	90.17	45.98	98.41	6.79	88.82	48.35	91.20	38.07
+ Energy	90.81	35.80	89.03	47.35	90.81	42.37	98.70	5.17	89.78	43.35	91.93	34.81
+ Mahalanobis	93.12	25.78	88.31	50.24	90.92	41.66	99.28	2.84	91.57	39.00	92.64	31.90
+ Residual	91.25	37.61	78.95	71.78	84.13	61.05	97.08	14.96	83.92	59.10	87.07	48.90
+ Vim	91.18	33.92	89.16	46.63	91.01	41.06	98.81	4.81	90.01	42.30	92.03	33.74
+ NECO	91.80	30.76	88.35	47.11	90.79	40.31	98.93	4.07	89.71	43.80	91.92	33.21
+ X-Maha (ours)	96.85	11.28	88.36	49.55	91.06	40.36	99.26	2.84	93.58	30.70	93.82	26.95
Adapter												
+ MSP	85.48	49.04	84.97	56.62	86.28	53.16	96.97	12.59	83.56	57.50	87.45	45.78
+ MLS	89.75	40.18	88.51	49.51	90.28	44.91	98.34	6.89	88.88	48.10	91.15	37.92
+ Energy	90.47	37.02	89.01	46.88	90.93	41.73	98.65	5.59	89.79	42.90	91.77	34.82
+ Mahalanobis	92.61	28.32	89.17	47.15	91.47	39.20	99.24	3.00	91.35	39.95	92.77	31.52
+ Residual	91.32	37.02	82.47	65.59	86.63	55.03	97.42	12.88	83.67	60.25	88.30	46.15
+ Vim	90.83	35.55	89.20	45.93	91.15	40.46	98.76	5.14	90.00	42.05	91.99	33.83
+ NECO	91.13	33.10	88.91	44.55	91.23	37.50	98.84	4.33	89.49	43.10	91.92	32.52
+ X-Maha (ours)	96.71	12.48	89.35	46.41	91.87	37.28	99.28	2.77	93.41	31.90	94.12	26.17
Full fine-tuning												
+ MSP	82.21	56.24	81.12	65.98	81.83	62.82	93.92	24.60	78.67	64.85	83.55	54.90
+ MLS	87.34	48.72	84.31	60.57	85.87	57.24	96.04	18.77	86.30	56.00	87.97	48.26
+ Energy	87.32	49.65	84.07	61.19	85.70	58.51	95.57	22.25	86.55	55.45	87.84	49.41
+ Mahalanobis	89.84	37.94	85.82	56.61	87.51	53.62	98.21	7.27	87.21	52.45	89.72	41.28
+ Residual	81.65	65.37	71.82	83.97	75.22	78.32	92.41	38.93	70.36	79.90	$\frac{39.72}{78.29}$	69.30
T INCSIQUAL												
	87.56	48.42	84.12	60.91	85.80	58.11	95.81	20.61	86.53	55.70	87.97	48.75
+ Vim + NECO	87.56 87.56	48.42 43.74	84.12 83.30	60.91 57.95	85.80 85.99	58.11 53.72	95.81 97.11	20.61 11.76	86.53 85.76	55.70 52.20	87.97 87.95	48.75 43.87